TURBULENT STATISTICS OF NEUTRALLY STRATIFIED FLOW WITHIN AND ABOVE A SPARSE FOREST FROM LARGE-EDDY SIMULATION AND FIELD OBSERVATIONS

HONG-BING SU[1,*], ROGER H. SHAW[1], KYAW THA PAW U[1], CHIN-HOH MOENG[2] and PETER P. SULLIVAN[2]

[1]*Atmospheric Science Program, University of California, Davis, California, USA*
[2]*National Center for Atmospheric Research, Boulder, Colorado, USA*

Abstract. Turbulent statistics of neutrally stratified shear-driven flow within and above a sparse forest canopy are presented from a large-eddy simulation (LES) and compared with those from observations within and above a deciduous forest with similar height and foliage density. First- and second-order moments from the LES agree with observations quite well. Third-order moments from the LES have the same sign and similar vertical patterns as those from the observations, but the LES yields smaller magnitudes of such higher-order moments. Turbulent spectra and cospectra from the LES agree well with observations above the forest. However, at the highest frequencies, the LES spectra have steeper slopes than observations. Quadrant and conditional analyses of the LES resolved-scale flow fields also agree with observations. For example, both LES and observation find that sweeps are more important than ejections for the transport of momentum within the forest, while inward and outward interaction contributions are both small, except near the forest floor. The inter-mittency of the transport of momentum and scalar increases with depth into the forest. Finally, ramp structures in the time series of a passive scalar at multiple levels within and above the forest show similar features to those measured from field towers. Two-dimensional (height-time cross-section) contours of the passive scalar and wind vectors show sweeps and ejections, and the characteristics of the static pressure perturbation near the ground resemble those deduced from field tower-based measurements. In spite of the limited grid resolution (2 m × 2 m × 2 m) and domain size (192 m × 192 m × 60 m) used in this LES, we demonstrate that the LES is capable of resolving the most important characteristics of the turbulent flow within and above a forest canopy.

1. Introduction

Large-eddy simulation (LES) directly computes the resolvable flow fields and para-meterizes the subgrid-scale (SGS) covariances and source/sink terms. It is assumed that the resolved motions contain most of the kinetic energy and transport most of the momentum and mass. Previous studies applying LES to the turbulent flow within and above a forest (Shaw and Schumann, 1992; Patton et al., 1994, 1995)

* *Current address*: Laboratory for Atmospheric and Environmental Physics, University of Georgia, Griffin, Georgia 30223-1797, USA. Email: hsu@gaes.griffin.peachnet.edu.

have shown that LES is able to reproduce many characteristics of the turbulent flow in this regime. For example, normalized profiles of mean longitudinal velocity, turbulent kinetic energy (TKE), and skewnesses of the longitudinal and vertical velocity components are similar to those from field measurements, especially within the forest.

Shaw and Schumann (1992) examined the effects of different leaf area indices on the turbulent statistics within and above a forest. They also included a prescribed heat source within the forest to study the buoyancy effect. Patton et al. (1995) studied the influence of canopy heterogeneity on TKE. One possible problem with these studies is that the simulated Reynolds stress decreased almost linearly from its maximum value at the top of the forest to zero at the top of the numerical domain, which was only three times the canopy height. However, field observations indicate a near-constant flux in the surface layer above the canopy (Kaimal and Finnigan, 1994). In addition, the LES of Shaw and Schumann (1992) showed that skewnesses of the longitudinal and vertical velocities reversed sign just above the forest, while observations have demonstrated that the change with height is not so rapid (Shaw and Seginer, 1987; Leclerc et al., 1991).

The present study focuses on neutrally stratified shear-driven flow within and above a sparse forest (LAI=2), because turbulent flow in the vicinity of a plant canopy is strongly shear-driven, and because of the availability of a suitable observational data set. The model forest is assumed to be horizontally uniform, and the vertical extent of the domain is three times the forest height as in Shaw and Schumann (1992) and Patton et al. (1994, 1995). However, an artificial momentum source has been added at the top of the domain to mimic the transport of momentum from a higher level to drive the flow at a lower level. This results in a constant flux layer above the forest which is consistent with field observations of atmospheric surface layer turbulence. It was thought that this change would have beneficial effects on the higher-order statistics.

Shaw and Schumann (1992) added an additional dissipation term in the SGS kinetic energy equation to account for the wake motions behind tree elements, and to increase the dissipation of kinetic energy within the forest because small eddies are expected to dissipate more rapidly than larger eddies. Kanda and Hino (1994) and Patton et al. (1995) included this additional dissipation term, but also examined the effects of wake production by adding a variable fraction of the resolved-scale kinetic energy loss due to the drag force into the SGS kinetic energy equation. A characteristic of the flow fields created is that the slope of the inertial subrange spectra of the simulated flow inside the canopy is much steeper than the observed "−5/3" slope from field measurements (e.g., Amiro, 1990).

In the present study, we include all the resolved-scale kinetic energy loss due to the drag force in the SGS kinetic energy equation. This leads to an SGS kinetic energy that is larger than in the case in which the wake production is excluded in the SGS TKE budget as in Shaw and Schumann (1992). Consequently, we modify the empirical constant used in the parameterization of the SGS eddy diffusivity

inside the forest, such that spectra exhibit a slope of the inertial subrange close to observed spectra within a forest.

In this paper, parameterizations of the subgrid covariances within the canopy, the upper boundary conditions and the major driving force of the whole system are described in Section 2. A brief description of the LES output, the experimental data and analysis methods is given in Section 3. A range of turbulent statistics are presented from both LES and measurement, and are compared in Section 4. These include vertical profiles of mean values, variances, covariances and skewnesses; spectra and cospectra; quadrant and conditional analyses. Signatures and some characteristics of coherent structures from the LES are also shown and compared with tower-based observations.

The main objective of this paper is to demonstrate that LES is able to reproduce the major characteristics of airflow in the vicinity of a forest canopy under neutral stratification, while a detailed examination of any one aspect of the LES results is not presented in this paper. It is thought that such extensive comparisons of single-point turbulent statistics from the LES with observations will provide confidence in applying the LES output for further analysis and improve our understanding of canopy dynamics (e.g., the role of static pressure perturbation, evaluation of closure schemes, space-time correlation analysis, vortical structure associated with coherent structures or sweeps/ejections). The set of statistics we chose for the comparisons have been well documented in many previous field and wind tunnel observations in defining turbulence characteristics within and immediately above a plant canopy.

2. Methodology

2.1. THE LARGE-EDDY SIMULATION

2.1.1. *The Governing Equations for the Resolved-Scale Flow Field*
For incompressible flow under neutral condition, the conservation equations for resolved-scale momentum, mass and a scalar can be written as follows.

$$\frac{\partial \langle u_i \rangle}{\partial t} = -\frac{\partial \langle u_i \rangle \langle u_j \rangle}{\partial x_j} - \frac{1}{\rho} \frac{\partial \langle p \rangle}{\partial x_i} - \frac{\partial \langle u_i'' u_j'' \rangle}{\partial x_j} + F_i \tag{1}$$

$$\frac{\partial \langle u_j \rangle}{\partial x_j} = 0 \tag{2}$$

$$\frac{\partial \langle \chi \rangle}{\partial t} = -\frac{\partial \langle \chi \rangle \langle u_j \rangle}{\partial x_j} - \frac{\partial \langle \chi'' u_j'' \rangle}{\partial x_j} + S_\chi \tag{3}$$

where the angle bracket indicates a grid-volume-averaging and the double prime denotes a deviation from such an averaged value; u_i is the velocity component

in the x_i-direction; p is static pressure; ρ is air density; χ represents the concentration of a passive scalar; and F_i denotes the drag force in the x_i-direction imposed by the tree elements. The term S_χ is the grid-volume-averaged source of scalar χ. The molecular diffusion terms have been assumed to be much smaller than turbulent diffusion and have therefore been neglected. The horizontal mean of the resolved-scale vertical velocity is set to zero as in Moeng (1984). Thus, the resolved vertical velocity represents a deviation from hydrostatic balance and any larger-scale motion that has a non-zero horizontal mean vertical velocity.

In this study, the passive scalar in Equation (3) is considered to be the water vapor mixing ratio but buoyancy effects due to vapor flux are ignored. In addition, we have not used a prescribed external large-scale pressure gradient force to drive the turbulent flow as in previous studies (Shaw and Schumann, 1992; Patton et al., 1994, 1995). Instead, we have added an artificial driving force at the top of the domain, as will be discussed in Section 2.2.

2.1.2. *Parameterizations of SGS Covariances and Sources/Sinks*

A local down-gradient diffusion scheme (Moeng, 1984) has been used to parameterize the SGS covariances,

$$\langle u_i'' u_j'' \rangle = \tau_{ij} + \frac{2}{3} \langle e'' \rangle \delta_{ij} = -\langle K_M \rangle \left(\frac{\partial \langle u_i \rangle}{\partial x_j} + \frac{\partial \langle u_j \rangle}{\partial x_i} \right) + \frac{2}{3} \langle e'' \rangle \delta_{ij} \qquad (4)$$

$$\langle \chi'' u_j'' \rangle = -\langle K_\chi \rangle \frac{\partial \langle \chi \rangle}{\partial x_j} \qquad (5)$$

where δ_{ij} is the Kronecker delta; $\langle K_M \rangle$ and $\langle K_\chi \rangle$ are the SGS eddy diffusivities for momentum and scalar χ, respectively. For neutrally stratified flow, we have used $\langle K_M \rangle = c_K \Delta \langle e'' \rangle^{1/2}$ and $\langle K_\chi \rangle = \langle K_M \rangle / S_C$. The subgrid length scale Δ is equal to $[(1.5\Delta x)(1.5\Delta y)\Delta z]^{1/3}$ with the grid spacing $\Delta x = \Delta y = \Delta z = 2$ m. The factor 1.5 appears due to the fact that the upper one-third of the wavenumbers are truncated to eliminate aliasing errors (Moeng and Wyngaard, 1988). The Schmidt number S_C is set to 0.33 as in Andrén et al. (1994) for a neutrally stratified PBL. The coefficient c_K will be discussed later.

A governing equation for the SGS kinetic energy $\langle e'' \rangle = \langle u_i'' u_i'' \rangle / 2$ is written,

$$\frac{\partial \langle e'' \rangle}{\partial t} = -\frac{\partial \langle u_j \rangle \langle e'' \rangle}{\partial x_j} - \langle u_i'' u_j'' \rangle \frac{\partial \langle u_i \rangle}{\partial x_j} - \frac{\partial \left\langle u_j'' \left(e'' + \frac{p''}{\rho} \right) \right\rangle}{\partial x_j} - \epsilon - \langle u_i \rangle F_i \quad (6)$$

where the terms on the right-hand side of Equation (6) represent, in order, advection of $\langle e'' \rangle$ by the resolved-scale flow, shear production, diffusion by SGS eddies, viscous dissipation, and wake production. This last term represents the transfer of resolved-scale kinetic energy into SGS kinetic energy by the pressure/form drag

imposed by the tree elements. Here we have assumed that viscous drag is negligible compared with form/pressure drag (Thom, 1975).

Moeng and Wyngaard (1988) parameterized the dissipation rate as $\epsilon = c_e \langle e'' \rangle^{3/2}/\Delta$ and derived the coefficient $c_e = 0.93$ using the inertial-subrange property of a "$-5/3$" spectral slope. They also expressed the SGS eddy diffusivity in Equation (4) as $\langle K_M \rangle = c_K \Delta \langle e'' \rangle^{1/2}$. To derive the coefficient c_K, they assumed a balance between shear production and viscous dissipation of SGS kinetic energy and obtained the coefficient $c_K = 0.1$.

However, we found that using $c_K = 0.1$ led to a slope of the inertial-subrange spectrum which ranged from -6 to -9, much steeper than "$-5/3$", inside the canopy. This is likely because, inside the canopy, we have included an additional wake production term in Equation (6), which turns out to be larger than shear production of SGS kinetic energy. Our tests with $c_K = 0.1$ demonstrated that, inside the forest, wake production was at least three times larger than shear production. A derivation for c_K similar to that of Moeng and Wyngaard (1988) requires not only the inertial-subrange "$-5/3$" spectrum but also a quantitative description of the lower wavenumber (large-scale) spectrum. This is because the canopy drag force acts on airflow motions of all scales and those large-scale eddies also contribute to the wake production of SGS kinetic energy.

Similar to Moeng and Wyngaard (1988), we assume a balance between shear production and viscous dissipation of the SGS kinetic energy and use $c_K = 0.1$ above the forest. However, inside the forest, a balance is assumed to be between shear production, wake production and viscous dissipation of the SGS kinetic energy. Since wake production is at least three times larger than shear production when $c_K = 0.1$ is used, and shear production is proportional to c_K, we reduce c_K to 0.025 inside the forest. We find that, using this value for c_K, the slope of the inertial-subrange spectrum is a much better approximation to the observed "$-5/3$", as we show later.

However, it is expected that the value of c_K determined by the above 'trial-and-error' method may vary with leaf area density. Therefore, an analytical and universal formula for estimating c_K should be further investigated, and factors such as leaf area density should be considered.

As pointed out in previous studies (Shaw and Seginer, 1985; Shaw and Schumann, 1992), small eddies dissipate much faster than large eddies. The pressure/form drag imposed by the canopy elements breaks down large eddies into small wake motions and therefore accelerates the dissipation of kinetic energy within a plant canopy. This is the so-called 'short-circuit effect'. In both Shaw and Schumann (1992) and the present study, the viscous dissipation rate ϵ is parameterized as proportional to $\langle e'' \rangle^{3/2}$. Inside the canopy, the present study includes a wake production term in the SGS kinetic energy equation and yields a larger SGS kinetic energy than the study presented by Shaw and Schumann (1992), which did not include such a term in the SGS TKE budget. Therefore, the parameterized viscous dissipation rate ϵ in the present study is larger than in Shaw and Schumann

(1992). Wake production is larger than shear production of SGS kinetic energy as discussed above, and therefore the above parameterization of ϵ and the addition of the wake production term in the SGS kinetic energy equation qualitatively reflects the 'short-circuit effect'.

Instead of including a wake production term in Equation (6), Shaw and Schumann (1992) added a second dissipation term $2\langle e'' \rangle / \tau$ to account for the additional dissipation rate of kinetic energy due to the wake motions behind tree elements, where τ was a time scale for the form/pressure drag. Kanda and Hino (1994) and Patton et al. (1995) included the above additional dissipation term but assumed that only a fraction, α ($0 \leq \alpha \leq 1$), of the wake production term in Equation (6) contributed to the SGS kinetic energy and that a portion $(1-\alpha)$ of the wake destruction of resolved-scale kinetic energy dissipated rapidly into internal energy. Tests demonstrated that the additional dissipation term (Shaw and Schumann, 1992) was substantially smaller than the viscous dissipation rate and had very little effect on turbulent statistics. Accordingly, we have not included the second dissipation term due to wake motions in the present study.

The grid-volume averaged pressure/form drag force in the x_i-direction F_i is parameterized as in Shaw and Schumann (1992).

$$F_i = -C_d a_L |\langle V \rangle| \langle u_i \rangle \tag{7}$$

where $C_d = 0.15$ is a constant drag coefficient as used by Shaw and Schumann (1992), and an estimate of C_d using measured mean longitudinal velocity and momentum flux within a deciduous forest will be shown later; a_L is the leaf area density which is assumed horizontally homogeneous but varying vertically (Figure 1a); $|\langle V \rangle| = (\langle u_i \rangle \langle u_i \rangle)^{1/2}$ is the scalar wind speed.

Within the canopy, the grid-volume-averaged source of the passive scalar S_χ must also be parameterized. In this study, the vertical profile of S_χ is set to match the source distribution of water vapor mixing ratio $S_q(z)$ from a study that links a coupled leaf and canopy model (Su et al., 1996) with the LES, as shown in Figure 1b. Source strength is assumed horizontally uniform and constant with time.

2.2. COMPUTATIONAL SPECIFICS

A pseudospectral method is used to evaluate horizontal derivatives, while a second-order centered finite difference is used to compute vertical derivatives (Moeng, 1984). A third-order Runge-Kutta scheme is used for time stepping (Spalart et al., 1991; Sullivan et al., 1996). A time interval may be determined by the maximum velocity component in the whole domain at each time step with a fixed Courant-Friedrichs-Lewy (CFL) number of 0.63. However, for the study presented here, a fixed time interval of 0.1s is used. This time interval is smaller than the time interval determined from the maximum velocity, the grid spacing and CFL = 0.63, but is consistent with the frequency of measured single-point time series data collected in the field measurements.
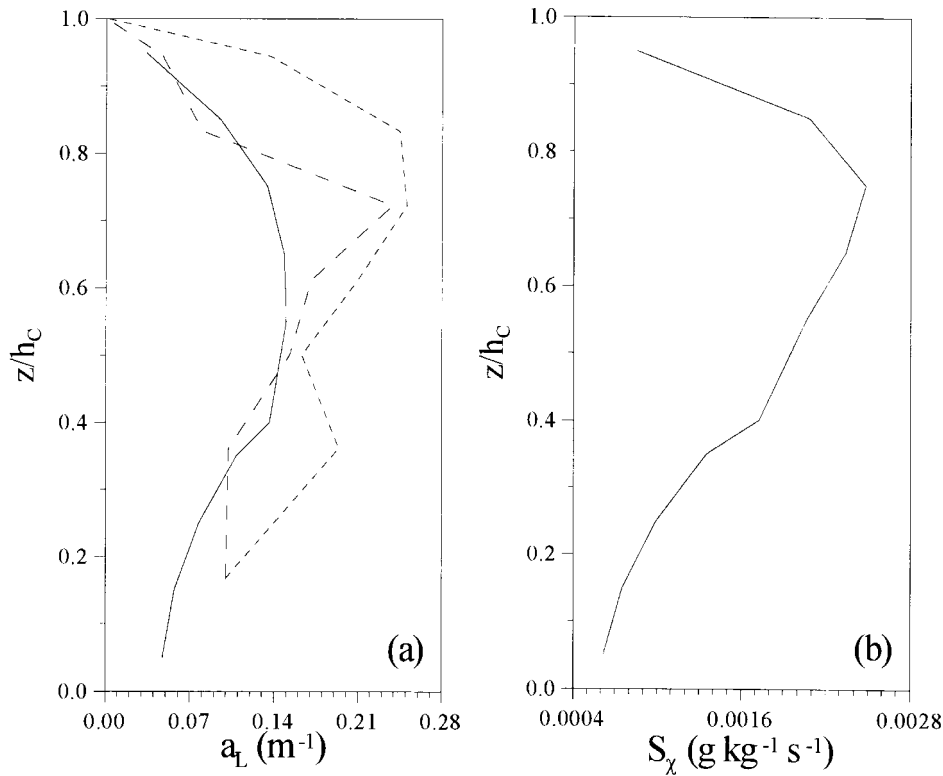
Figure 1. (a) leaf area density a_L (solid curve: used in the LES with a leaf area index LAI = 2, short (LAI = 2.57) and long (LAI = 2.08) dashed curves: measured within the Camp Borden deciduous forest on day 274 and 281, 1986, respectively (Neumann et al., 1989); and (b) horizontally uniform source of the scalar (water vapor mixing ratio).

The domain size and grid spacing are the same as those used in previous work (Patton et al., 1994, 1995), i.e., 96 × 96 × 30 grid points in the x, y and z directions with equal grid spacing of 2 m. The forest height h_C is set to 20 m, and the same horizontally homogeneous leaf area density profile (LAI = 2) as in Shaw and Schumann (1992) is used (Figure 1a).

The lateral boundary conditions are periodic, and the lower boundary condition is rigid and no-slip. The horizontal wind velocity components at the first grid point from the surface and a logarithmic wind profile are used to estimate the local friction velocity and the SGS stresses at the surface with a prescribed surface roughness length ($z_{0,S}$ = 0.05 m). The SGS flux of the passive scalar at the surface is set to zero, which implies a zero local vertical gradient of the resolved-scale concentration of the scalar at the surface.

The upper boundary is treated as a frictionless and rigid lid. Thus, the resolved-scale fluxes of momentum and the passive scalar are zero at the upper boundary. However, there is a passive scalar source within the forest canopy which occu-

pies one-third of the whole domain in the vertical. In order to conserve the total amount of the scalar and obtain steady-state statistics, we have added a horizontally uniform SGS scalar sink in the top layer ($iz = 30$) to remove the total scalar produced by the source within the canopy. The total sink balances the total source of the scalar. Therefore, the scalar concentration of the entire domain is a conserved quantity with time.

To mimic the transfer of momentum from above as a driving force for the flow at lower levels, there are various options. One is to specify a constant mean longitudinal velocity at the top of the domain. An alternative method is similar to the treatment of the scalar concentration, i.e., to conserve the total momentum of the domain, at each time step, an artificial driving force is uniformly added at the top of the domain. The total magnitude of this driving force is set equal to the sum of the form drag induced by the canopy elements and the friction at the soil surface. For the study presented here, the latter is used as the only driving force of the turbulence flow, and the horizontal mean pressure gradient is set to zero.

Other details regarding the numerics in the LES code can be found in Moeng (1984), Moeng and Wyngaard (1988) and Sullivan et al. (1996).

3. Data Analyses

3.1. LES OUTPUT

Three-dimensional data sets at selected time steps and time series at selected locations were saved from the LES after the flow reached an equilibrium state. In particular, three dimensional data sets were saved every 30-s over a period of 20-min real time. Time series of a single $y - z$ slice located at the center of the domain ($ix = 49$) and of a single $x - z$ slice centered at $iy = 49$ were saved at a sampling frequency of 1 Hz.

3.2. EXPERIMENTAL DATA

Turbulence data of velocities and temperature fluctuations were collected at 10 Hz from ultrasonic anemometer-thermometers (Kaijo Denki Co., Ltd.) positioned at seven heights on two scaffolding-type towers within and above a deciduous forest near the northern perimeter of the Camp Borden military base in Ontario, Canada during September and October, 1986. Detailed descriptions of the site and experiment can be found in Shaw et al. (1988). The average height of the forest was about 18 m, which is close to the height of the model forest in our LES. Leaf area indices were estimated by collection of naturally falling leaves in a series of bushel baskets placed at the ground level. Back calculation from the measured areas of harvested leaves showed that LAI was about 2 in early October (Shaw et al., 1988). Data used in this study were selected from day 275 (October 2), day 280 (October 7) and day 281 (October 8) when the wind came from directions with

sufficient upwind fetch, and at the same time, all measurement sensors worked properly. Leaf area density profiles estimated from hemispherical photographs and a Markov model (Neumann et al., 1989) for day 274 (LAI = 2.57) and day 281 (LAI = 2.08) are given in Figure 1a. The latter appears to be closer to the model forest than the former.

Results of analyses presented here that only require velocities are based on five 30-min periods of data during day 280 and 281 under near-neutral conditions ($-0.05 < h_C/L < -0.01$), where L is the Obukhov length calculated at the top of the forest. Because temperature fluctuations were measured at all seven heights while humidity observations were more limited, analyses that also require measurement of scalar fluctuations are based on four 30-min periods of data of velocity and temperature fluctuations during day 275 under unstable conditions ($-0.16 < h_C/L < -0.11$). Repeated ramp structures are evident at all heights in the time series of these temperature data as shown in previous studies (Gao et al., 1989).

3.3. ANALYTICAL PROCEDURES

As usual, turbulent statistics based upon the field measurements are computed from single-point time averaging. A coordinate rotation has also been performed to force the local mean lateral and vertical velocities of each 30-min period to zero. From the LES output, we have computed turbulent statistics using both horizontal and time averaging procedures. A mean value is obtained from either horizontal averaging (over all x and y locations of the same z) or time averaging at a single point, and is indicated by an overbar. A departure from the horizontal mean or the single-point time average is denoted by a single prime. In addition, for horizontal averaging, quantities are further averaged over the 40 samples collected during the 20-min period. Similarly, single-point time averaged quantities are further averaged over the 96 locations in the lateral (y) direction.

The artificial driving force of momentum and the scalar sink added in the top layer to conserve the total momentum and scalar over the entire domain of the LES, lead to relatively constant vertical fluxes of momentum and scalar above the canopy as shown later. As a consequence, however, the vertical gradients of mean longitudinal velocity and scalar concentration are very large between the top two grid points. These large mean gradients decrease quickly within the top five grid points. This is because of the rigid upper boundary that limits the mixing length or eddy size and so the efficiency of mixing, as is typically the case in near-wall flows. As a result, we only show flow and scalar statistics up to twice the canopy height. We note that most field tower measurements extend to levels approximately twice the canopy height. In addition, we find that turbulent statistics computed from time averaging are very close to those from horizontal averaging using the LES output. Therefore, only the latter are presented in the following, except for the spectral analyses.

4. Results and Discussion

4.1. VERTICAL PROFILES

4.1.1. *Mean Longitudinal Velocity and Scalar Concentration*

It is shown in Figure 2a that the normalized mean longitudinal velocity from LES matches the observation quite well in the upper forest. However, measured velocities are slightly lower in the middle and lower forest as well as at about twice the canopy height. The relative difference is largest in the lower forest because of lower mean velocity. The LES profile demonstrates strong shear and an inflection point near the top of the forest, similar to mean wind profiles observed in both wind tunnel and field measurements (Raupach et al., 1986; Gao et al., 1989; Kaimal and Finnigan, 1994). Figure 2b shows that the mean scalar concentration also has a weak inflection point near the top of the canopy.

In the inertial layer above a plant canopy under neutral condition, a logarithmic wind profile can be written as:

$$\overline{\langle u \rangle}(z) = \frac{u_*}{\kappa} \ln \left(\frac{z - d}{z_0} \right) \tag{8}$$

where $\kappa = 0.4$ is the von Karman constant; u_* the friction velocity; z the distance from the soil surface; d the zero-displacement height and z_0 the roughness length.

An independent estimate of the zero-plane displacement is the level at which the mean drag appears to act or the mean level of momentum absorption (Thom, 1971; Jackson, 1981; Raupach et al., 1986; Brunet et al., 1994). This can be written as the following:

$$d = \frac{\int_0^{h_C} z \bar{F}_1 \, dz}{\int_0^{h_C} \bar{F}_1 \, dz} = \frac{\int_0^{h_C} z \frac{d\overline{u'w'}}{dz} dz}{\int_0^{h_C} \frac{d\overline{u'w'}}{dz} dz} \approx h_C - \frac{1}{u_*^2} \int_0^{h_C} \overline{u'w'} \, dz \tag{9}$$

where the approximation is based upon the assumption that the momentum flux at the soil surface is negligible compared to the momentum flux at the top of the forest. Using Equation (9) with $u_* = 0.27$ m s^{-1} and the total kinematic momentum flux inside the forest as discussed later (Figure 4a), we obtain $d = 14.0$ m and $d / h_C = 0.70$, close to the average value of 0.75 measured over a wide range of natural canopies (Kaimal and Finnigan, 1994).

It should be noted that the logarithmic wind profile is only applicable in the inertial sublayer. In a manner similar to Raupach et al. (1986), we have plotted the mean longitudinal velocity versus the natural logarithmic function of $z - d$, i.e., $\ln(z - d)$, in Figure 3a. The straight line represents the logarithmic wind profile using $d = 14.0$ m, $u_* = 0.27$ m s^{-1} and a roughness length $z_0 = 1.9$ m.
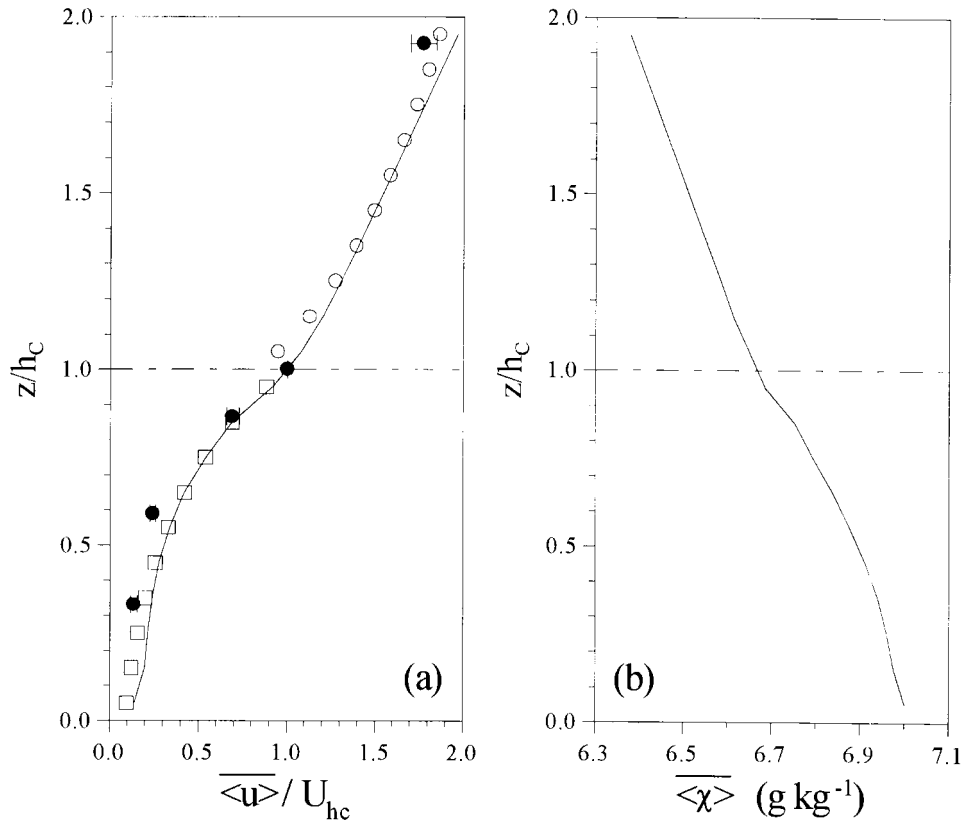
Figure 2. (a) mean longitudinal velocity normalized by the value at the top of the forest U_{hc}; (b) mean scalar concentration. The solid curves are from LES and the solid circles are from observation. In (a), the open circles above the forest represent a logarithmic wind profile from Equation (8) with $d = 14.0$ m, $u_* = 0.27$ m s^{-1} and $z_0 = 1.9$ m; and the open squares inside the forest represent an exponential wind profile from Equation (10) with $\nu_e = 2.48$ and $U_{hc} = 0.95$ m s^{-1}.

The value of z_0 is obtained by making the straight line tangential to the simulated mean longitudinal velocity profile.

Both Figures 2a and 3a suggest a thin inertial sublayer between $z = 1.35h_C$ or $\ln(z-d) = 2.56$ and $z = 1.55h_C$ or $\ln(z-d) = 2.83$, where the mean longitudinal velocity appears to obey the logarithmic law. Between $z = h_C$ and $z = 1.35h_C$ is the so-called roughness sublayer in which the flow does not obey surface layer similarity, and the logarithmic law. The fact that the simulated mean longitudinal velocity deviates from the logarithmic wind profile above $z = 1.55h_C$ is likely due to the limited vertical extent of the domain and the artificial momentum source added in the top layer in our LES. In addition, at about twice the canopy height, the observed mean longitudinal velocity is closer to the logarithmic wind profile than that from the LES.
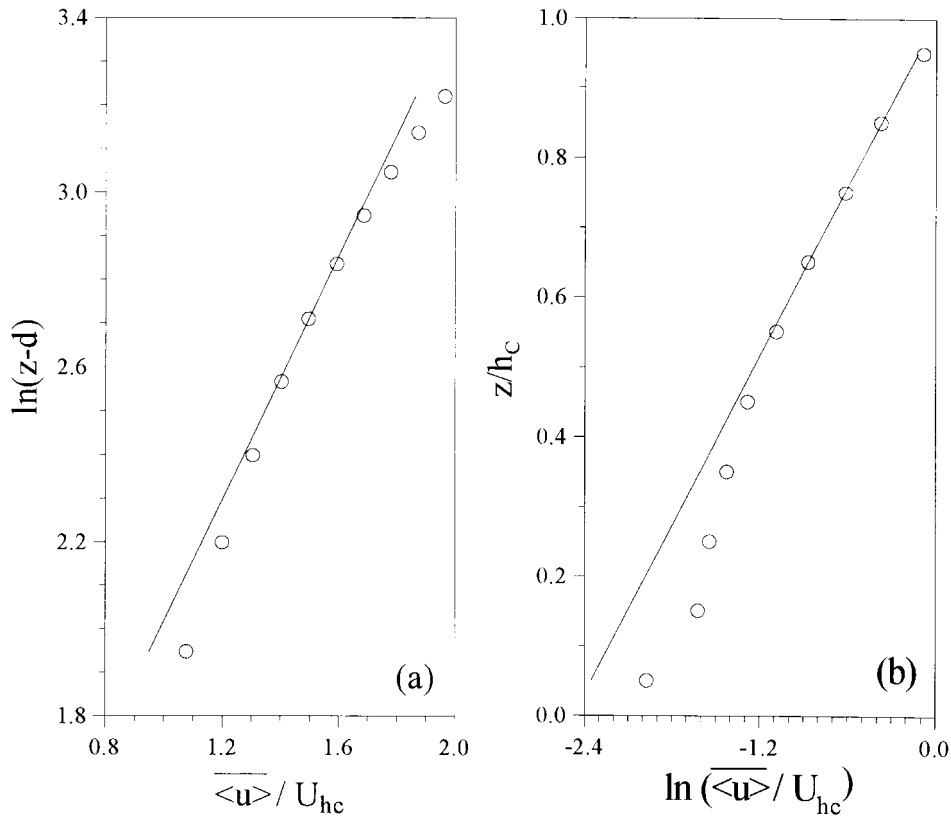
Figure 3. Solid lines: (a) normalized logarithmic wind profile above the forest [Equation (8)]; (b) normalized exponential wind profile within the forest [Equation (10)]; open circles: from LES.

Within the canopy, the mean longitudinal profile can be approximated by an exponential formula (Inoue, 1963; Cionco, 1965; Kaimal and Finnigan, 1994),

$$\overline{\langle u \rangle}(z) = U_{hc} \exp\left[-\nu_e \left(1 - \frac{z}{h_C} \right) \right] \tag{10}$$

where ν_e is an extinction coefficient.

It is shown in Figure 3b that $\ln(\overline{\langle u \rangle}(z)/U_{hc})$ is not a linear function of z/h_C, as implied by Equation (10); in particular the slope ν_e between 0.95 h_C and 0.55 h_C is quite different from that between 0.45 h_C and 0.15 h_C. A linear regression between 0.85 h_C and 0.65 h_C yields a slope $\nu_e = 2.48$, which falls in the range of 1.7–3.2 estimated from three different forest canopies with LAI from 1.0 to 4.0 (Kaimal and Finnigan, 1994). The exponential wind profile within the forest shown by open squares in Figure 2a is calculated from Equation (10) with $U_{hc} = 0.95$ m s^{-1} and $\nu_e = 2.48$, and fits the simulated mean longitudinal velocity profile quite well in the upper part of the forest, but shows relatively larger difference in the lower part
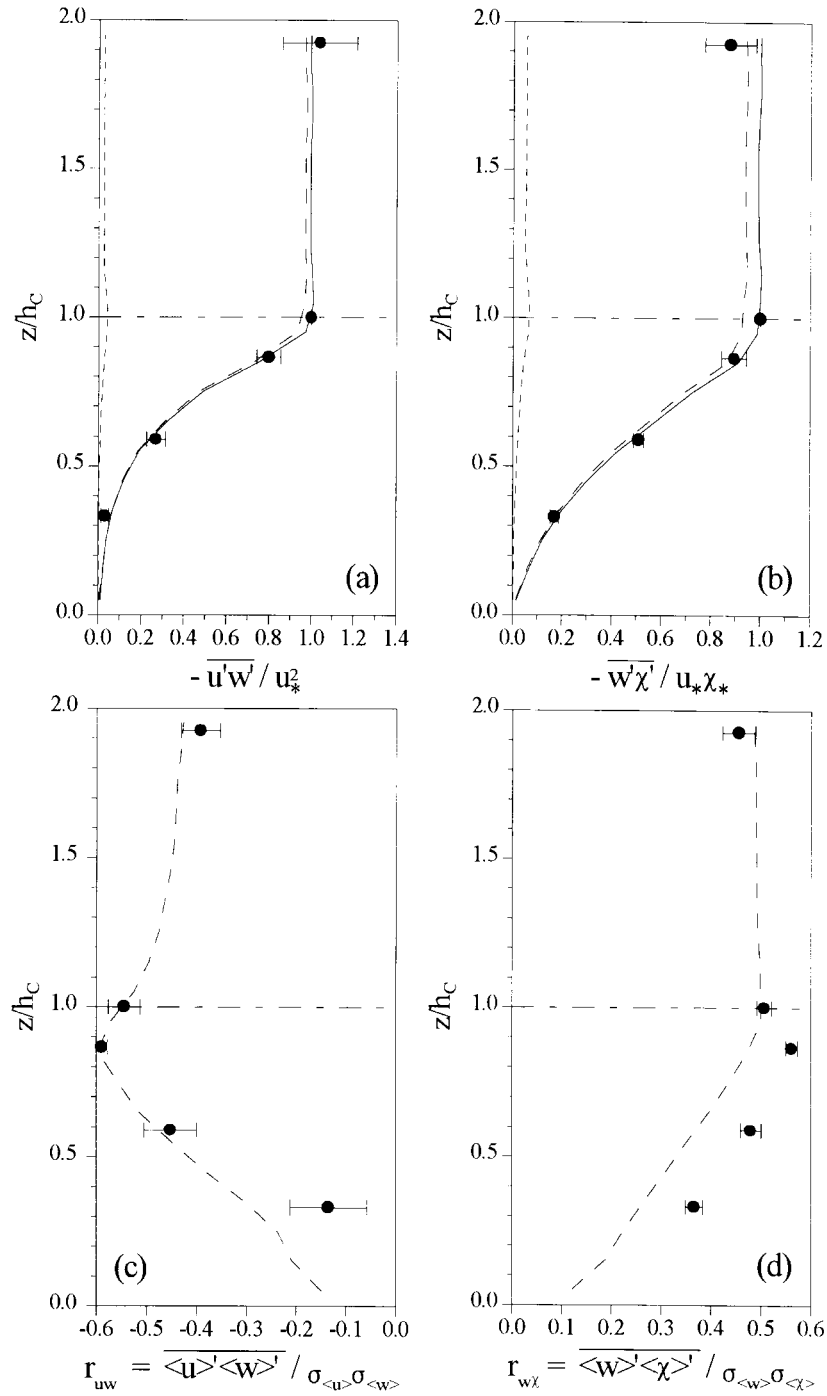
Figure 4. (a) Momentum flux normalized by $-u_*^2$; (b) scalar flux normalized by $-u_*\chi_*$; (c) correlation coefficient r_{uw}; (d) correlation coefficient $r_{w\chi}$. Curves are from LES (solid: total; long dashed: resolved-scale; short dashed: SGS) and solid circles are from observations.

of the forest, which is expected because ν_e is obtained from a regression between 0.85 h_C and 0.65 h_C.

4.1.2. *Kinematic Fluxes (Covariances) and Correlation Coefficients*

The LES yields an average friction velocity $u_* = 0.27$ m s^{-1} and a characteristic scalar $\chi_* = -0.12$ g kg^{-1} between h_C and 2 h_C, where $u_* = (-\overline{u'w'})^{1/2} = (-\overline{\langle u \rangle'\langle w \rangle'} - \overline{\langle u''w''\rangle})^{1/2}$ and $\chi_* = -\overline{w'\chi'}/u_* = -(\overline{\langle w \rangle'\langle \chi \rangle'} + \overline{\langle w''\chi''\rangle})/u_*$. Thus negative χ_* represents a positive (upward) flux of scalar. In the field measurements, u_* and χ_* are calculated at the top of the forest.

It is illustrated in Figures 4a and 4b that normalized kinematic vertical fluxes for u-momentum and the scalar are quite constant above the forest but decrease quickly with depth into the forest, and both match observation quite well. Averaged over a horizontal slice, constant fluxes of momentum and scalar above the forest are expected from our LES because there is no mean pressure gradient, nor is there a source or sink of scalar between the forest and the top layer of the domain.

In Figure 4c, it is also shown that the correlation coefficient r_{uw} between the longitudinal and vertical velocities from the LES also matches observation well in the upper half of the forest and above, while observation shows smaller values in the lower forest. There is a peak value of about -0.6 near 0.85 h_C, and the magnitude of the correlation decreases to a value between -0.4 and -0.45 above 1.5 h_C. In the upper part of the forest, the longitudinal and vertical velocities remain strongly correlated ($r_{uw} < -0.45$), while r_{uw} increases to about -0.14 at $z = 0.05$ h_C.

Similarly in Figure 4d, it is shown that the correlation coefficient $r_{w\chi}$ between vertical velocity and the scalar from the LES matches observation well above the canopy with a value of about 0.5, but is smaller than observation by about 0.1 inside the canopy. In addition, $r_{w\chi}$ from both LES and observation decreases with depth into the forest at about the same rate. However, LES does not show a distinct peak at 0.88 h_C as does the measurement.

4.1.3. *Turbulent Kinetic Energy (TKE)*

It is shown in Figure 5a that within the forest, the normalized TKE from the LES is slightly larger than observation, especially in the upper half of the forest. This perhaps indicates that the large percentage of SGS TKE within the canopy (up to 44% at $z/h_C = 0.65$) from the LES (Figure 5b) may not be realistic. The inclusion of an additional dissipation term in Equation (6), as proposed by Shaw and Schumann (1992), would have the effect of reducing the magnitude of SGS TKE, assuming the total dissipation of TKE does not change. Despite the relative large SGS contribution to TKE, Figure 5b shows that the parameterized SGS fluxes of momentum and the scalar account for less than 6% of the total fluxes, except for the first grid from the ground. This is because of the small length scale associated with SGS turbulence.
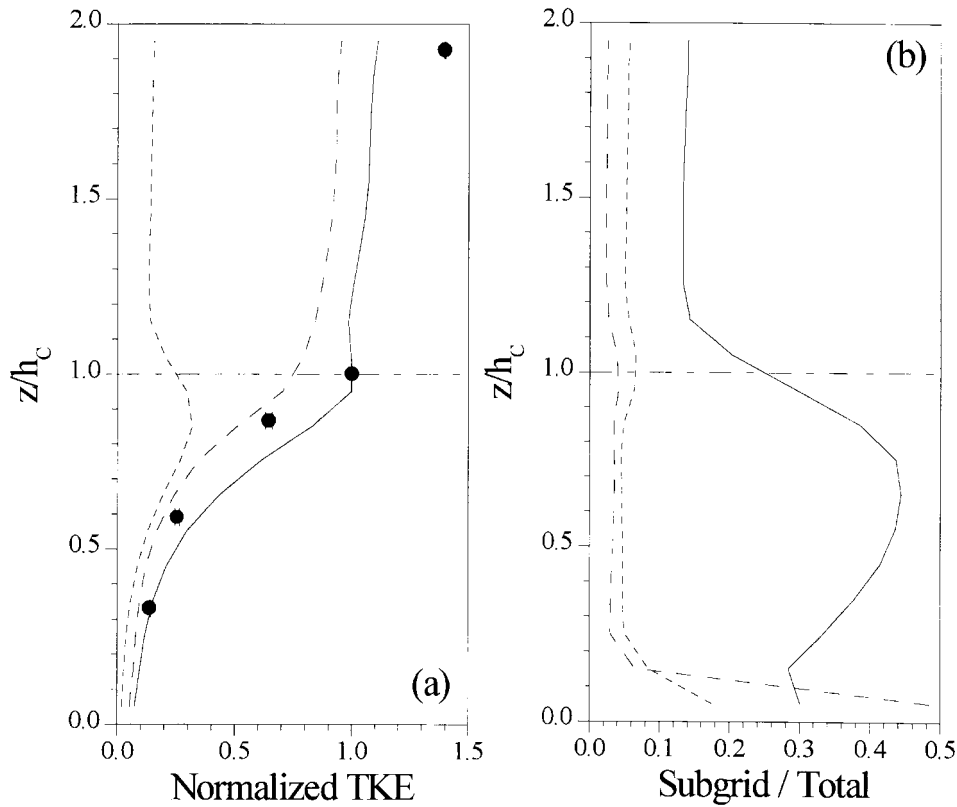
Figure 5. (a) TKE normalized by the value at the top of the forest (solid curve: total; long dashed curve: resolved-scale; short dashed curve: SGS; solid circles: observation); and (b) ratio of SGS portion to the total of TKE (solid curve), momentum flux (long dashed curve) and scalar flux (short dashed curve) from the LES.

4.1.4. *Variances*

It is shown in Figure 6a that the standard deviations of $\langle u \rangle$, $\langle v \rangle$ and $\langle w \rangle$ normalized by u_* are relatively constant from 1.2 h_C to 2 h_C but decrease quickly with depth into the canopy. It is clear that the LES and measurements agree quite well, although the LES yields slightly smaller magnitudes above the forest than the measurement.

Shown in Figure 6b are the vertical profiles of the relative turbulent intensity in the x, y and z directions, which are defined as the corresponding velocity standard deviations normalized by the mean longitudinal wind velocity at the same height. In general, LES yields a smaller relative turbulent intensity than the observation, especially with depth into the forest. This is partly a consequence of the fact that LES yields higher mean longitudinal velocity than the observation (Figure 2a). Within the forest, both LES and observation show that the relative turbulent inten-
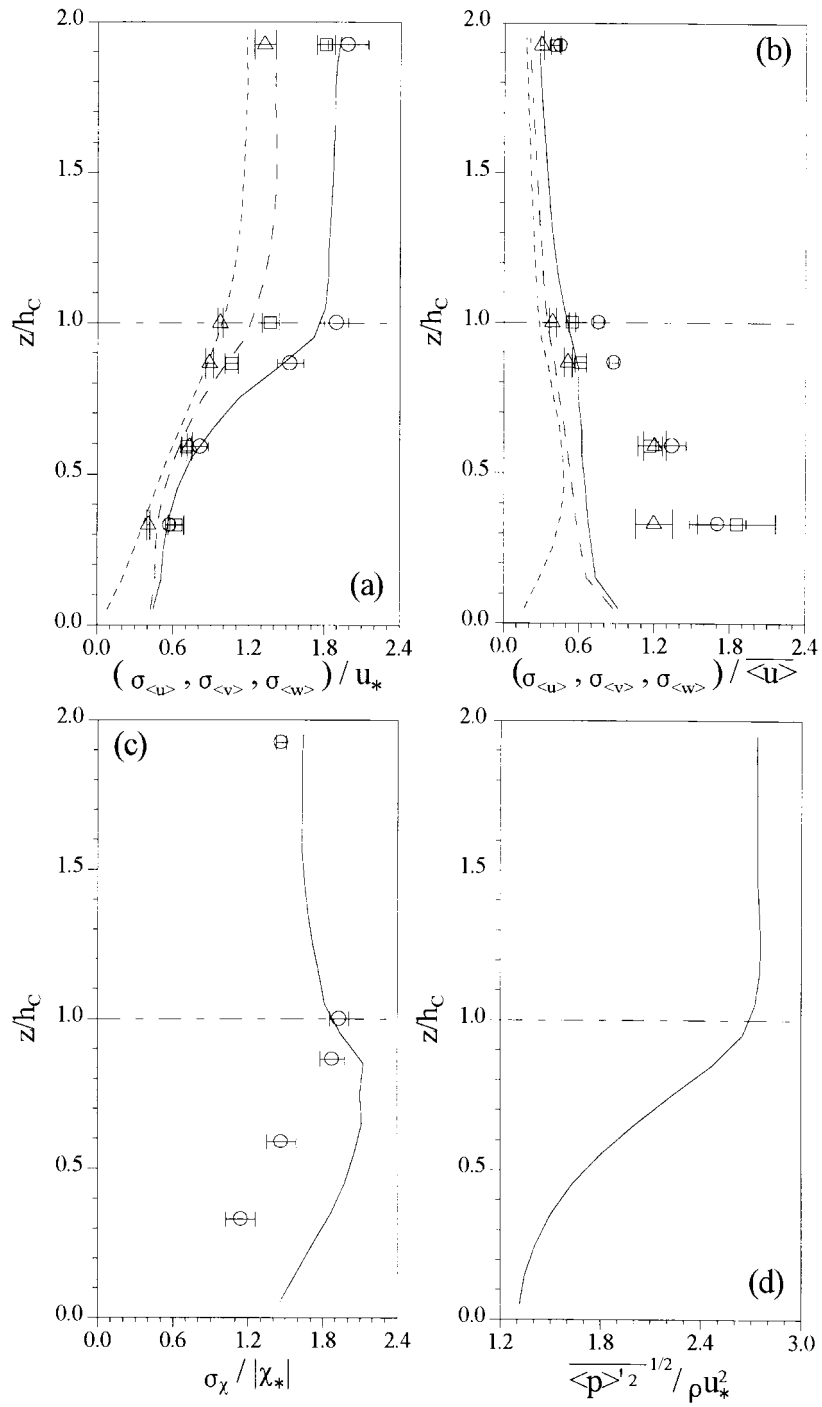
Figure 6. (a) Standard deviations of velocity components normalized by u_*; curves are from LES (solid: $\langle u \rangle$, long dashed: $\langle v \rangle$ and short dashed: $\langle w \rangle$) and points are from the observation (circle: u, square: v and triangle: w); (b) same as (a) but of relative turbulent intensity; (c) standard deviation of the scalar normalized by $|\chi_*|$ (curve: LES, open circle: observation); (d) standard deviation of kinematic static pressure normalized by u_*^2 from LES.
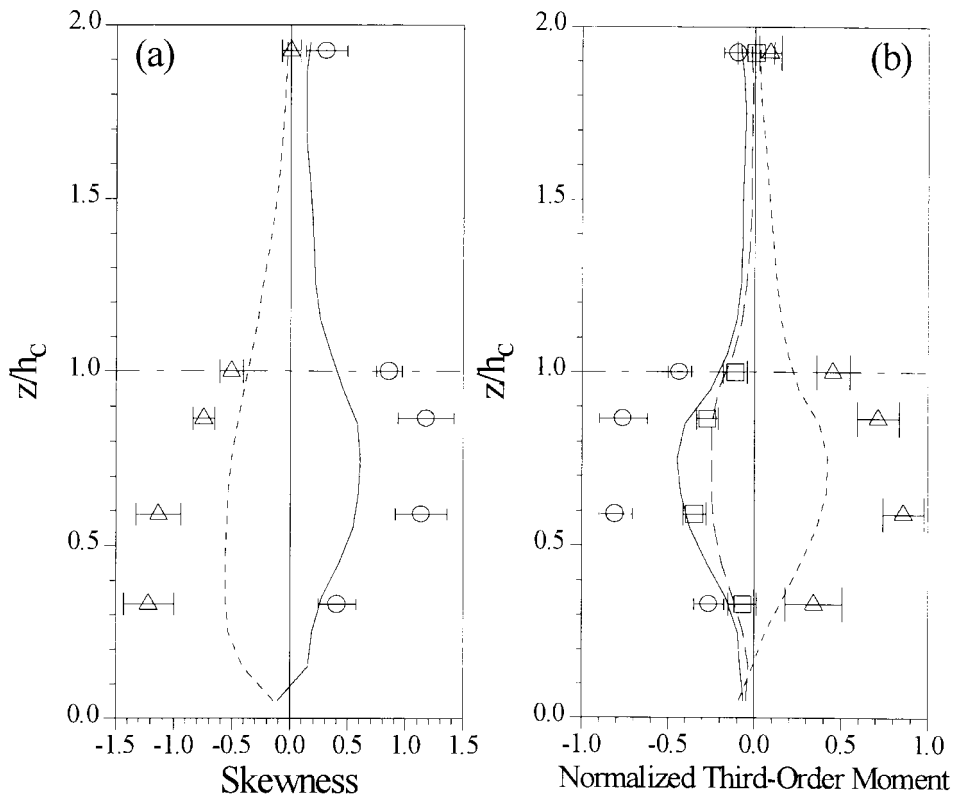
Figure 7. (a) Skewnesses of longitudinal velocity (solid curve or circle) and vertical velocity (short dashed curve or triangle); (b) mixed third-order moments normalized by corresponding standard deviations: $\overline{\langle u \rangle'^2 \langle w \rangle'}$ (solid curve or circle); $\overline{\langle v \rangle'^2 \langle w \rangle'}$ (long dashed curve or square) and $\overline{\langle u \rangle' \langle w \rangle'^2}$ (short dashed curve or triangle). Curves are from the LES and points are from the observation.

sity in the vertical direction has a peak near the middle of the forest, while those in the longitudinal and lateral directions continue to increase with decreasing height.

It is shown in Figure 6c that the normalized standard deviation of the scalar concentration from the LES is larger than the observation both within and above the forest. However, both LES and observation show that the normalized standard deviation decreases with depth into the forest.

In Figure 6d, it is illustrated that the normalized standard deviation of the kinematic static pressure is quite constant above the canopy with a value of about 2.9 but decreases quickly with depth into the forest. Observations of vertical profiles of the standard deviations of static pressure perturbations are not available for a comparison with Figure 6d.

4.1.5. *Third-Order Moments*

In Figure 7a, it is demonstrated that skewnesses of the longitudinal and vertical velocities from LES have the same sign and vertical trend as those from observations. For example, the longitudinal velocity is strongly positively skewed inside the forest (except for the first grid point from the soil surface) with a peak in the upper part of the canopy. Vertical velocity, on the other hand, is strongly negatively skewed within the canopy with no prominent peak. In addition, the magnitudes of the skewnesses decrease with increasing height above the forest, and the skewness of longitudinal velocity remains positive up to twice the forest height, while the skewness of vertical velocity reverses near twice the canopy height (at $z = 2.25\,h_C$ in the LES and not included in Figure 7a). This agreement is an improvement in the current LES compared to the LES by Shaw and Schumann (1992), where the reversals of sign appeared just above the forest. This is probably due to the artificial momentum source we have added in our LES and the more realistic vertical profiles of the second moments that this action creates. Skewness of the lateral velocity from both LES and measurement is very close to zero and is thus not shown.

Inside the canopy, the magnitudes of the skewnesses from the LES are only about 50% of those from observation. This is perhaps due to the limited grid resolution and vertical domain size in our LES. For example, Moeng and Wyngaard (1989) demonstrated that a finer resolution generally yielded much larger magnitudes of the third-order moments from their LES of the convective planetary boundary layer.

Similarly, Figure 7b demonstrates that three mixed third-order moments $\overline{\langle u \rangle'^2 \langle w \rangle'}$, $\overline{\langle v \rangle'^2 \langle w \rangle'}$ and $\overline{\langle u \rangle' \langle w \rangle'^2}$ normalized by corresponding standard deviations of velocities from the LES also have the same sign and vertical trends as those from observation. Both LES and measurement show that normalized $\overline{\langle u \rangle'^2 \langle w \rangle'}$ is more negative than normalized $\overline{\langle v \rangle'^2 \langle w \rangle'}$ within the forest. Again, inside the forest, the magnitudes of normalized $\overline{\langle u \rangle'^2 \langle w \rangle'}$ and $\overline{\langle u \rangle' \langle w \rangle'^2}$ from LES are only about half of those from observation, while LES and measurement yield similar magnitude of normalized $\overline{\langle v \rangle'^2 \langle w \rangle'}$.

4.1.6. *Mean Drag Force and Drag Coefficient*

Many closure models applied to the turbulent flow within plant canopies have included the following relationship between the vertical gradient of the horizontally averaged Reynolds stress and the horizontal mean drag force (Wilson and Shaw, 1977; Meyers and Paw U, 1986, 1987).

$$-\frac{\partial \overline{u'w'}}{\partial z} = -\bar{F}_1 \doteq C_D a_L \overline{\langle u \rangle}^2. \tag{11}$$

In the LES presented here as well as previous LES work (Shaw and Schumann, 1992), the subgrid-volume-averaged drag force is parameterized as Equation (7). By decomposing the resolved-scale velocity components into their horizontal mean

values and deviations from corresponding horizontal means, using a Taylor expansion and keeping the second-order terms, and horizontally averaging Equation (7), we obtain the following relationship between the horizontally-averaged drag force and the horizontal mean velocity components and their variances.

$$-\frac{\partial \overline{u'w'}}{\partial z} = -\bar{F}_1 \doteq C_d a_L [\overline{\langle u \rangle}^2 + \overline{\langle u \rangle'^2} + 0.5(\overline{\langle v \rangle'^2} + \overline{\langle w \rangle'^2})]. \tag{12}$$

In Equations (11) and (12), the first equal sign from the left is based on the assumption that the mean longitudinal momentum is conserved when the flow reaches an equilibrium state so that the vertical gradient of the Reynolds stress $-\partial \overline{u'w'}/\partial z$ is balanced by the horizontal mean drag force $\bar{F}_1$. We examined this assumption by comparing directly calculated $-\partial \overline{u'w'}/\partial z$ and $\bar{F}_1$ from our LES and found that they are very close to each other at all levels within the canopy (the result is not shown here for the sake of brevity). This is expected because the flow reached equilibrium state.

The far right-hand sides in Equations (11) and (12) are parameterizations or approximations of the horizontal mean drag force $\bar{F}_1$. It is noted that the drag coefficient C_d used in Equation (12) should be smaller than the drag coefficient C_D in Equation (11) because of the additional velocity variances in Equation (12).

In Figure 8a, it is demonstrated that momentum balance is well satisfied by the resolved-scale flow field at all nine heights within the forest, and implies that the far right-hand side in Equation (12) is a close approximation to the horizontal mean drag force $\bar{F}_1$. Using the far right-hand side in Equation (11) with $C_D = C_d = 0.15$, the mean drag $\bar{F}_1$ is underestimated by about 35% unless the drag coefficient C_D is increased by an equal amount.

When vertical profiles of both the Reynolds stress and mean wind speed are simultaneously measured in a wind tunnel or field experiment, drag coefficients can be estimated using the relationships given by Equations (11) and (12). It is noted that Equation (11) should be used to derive the drag coefficient used in closure models which employ Equation (11), while Equation (12) should be used to estimate the drag coefficient for studies such as the work presented here. For example, we have calculated the drag coefficient C_d using the measured mean longitudinal velocity, momentum flux and velocity variances using Equation (12), and the result is given in Figure 8b. The average value of C_d at the two heights in Figure 8b is 0.145, which provides justification for the value of 0.15 used in the LES.

4.1.7. *Eddy Diffusivities*

K-theory models applied to the turbulent flow within and above a plant canopy normally parameterize the eddy diffusivity as the product of a characteristic velocity scale and a mixing length. Using the following expressions for local down-gradient transport, along with the profiles of horizontally averaged momentum and scalar fluxes, mean longitudinal velocity and scalar concentration, we estimate the eddy diffusivities for momentum K_M and for scalar K_χ,
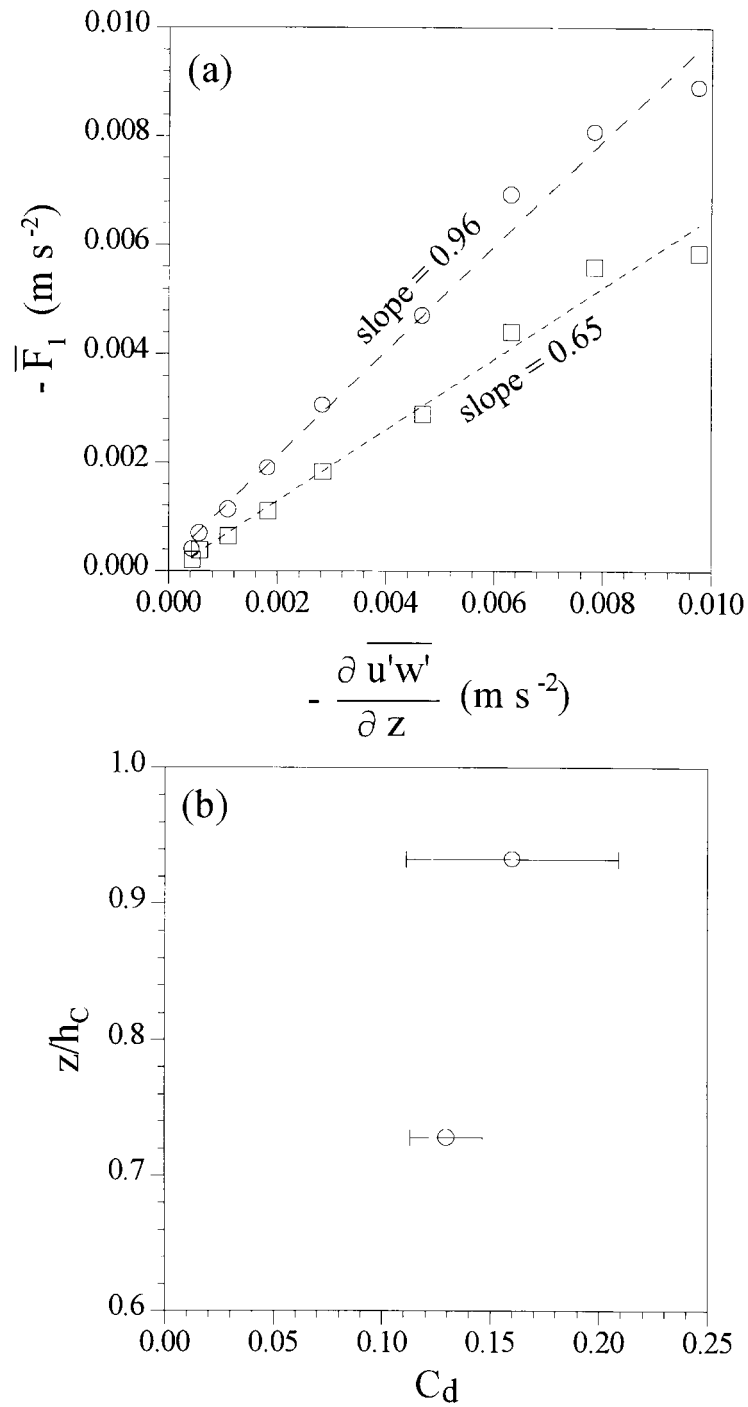
Figure 8. (a) The horizontal mean drag force $\bar{F}_1$ versus the vertical gradient of the Reynolds stress $\partial \overline{u'w'}/\partial z$, where $\bar{F}_1$ is approximated by the far right-hand sides in Equations (12) (circle) and (11) (square) with $C_d = C_D = 0.15$, respectively. The solid and dashed lines are corresponding linear regressions. Each point represents a height within the forest. (b) C_d estimated from Equation (12) using measured velocity data.
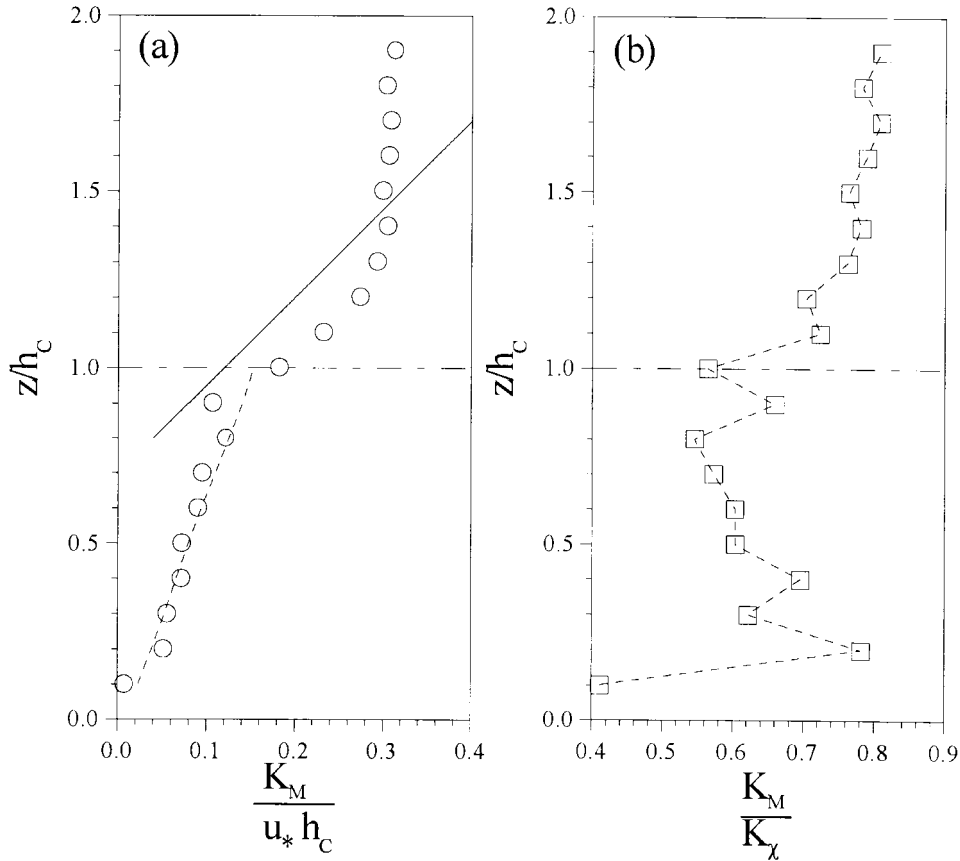
Figure 9. (a) Horizontal mean eddy diffusivities: open circles: calculated from Equation (13) using the LES; solid straight line: inertial sublayer eddy diffusivity $K^* = \kappa u_*(z - d)$; short dashed line: $L\sigma_w$ with $L = 3.1$ m and σ_w given in Figure 6a; (b) the ratio K_M/K_χ.

$$\overline{u'w'} = -K_M \frac{\partial \overline{\langle u \rangle}}{\partial z} \tag{13}$$

$$\overline{w'\chi'} = -K_\chi \frac{\partial \overline{\langle \chi \rangle}}{\partial z}. \tag{14}$$

It is shown in Figure 9a that the vertical gradient of K_M between 0.2 h_C and 0.8 h_C is less than half of that between h_C and 1.3 h_C. The roughness sublayer is evident as a region between $z = h_C$ and $z = 1.3\ h_C$, in which K_M is enhanced above its inertial sublayer value $K^* = \kappa u_*(z - d)$ which is shown as the solid line. At $z = h_C$, K_M is approximately 1.5 K^*. Both field (Raupach, 1979; Denmead and Bradley, 1985) and wind tunnel (Raupach et al., 1986; Brunet et al., 1994) observations have shown eddy diffusivity enhancement on the same order in the roughness sublayer. As discussed in Section 4.1.1, the simulated mean longitudinal

velocity profile does not obey the logarithmic law in the same region (Figures 2a, 3a). The nonlinear shape of K_M in the roughness sublayer seems to indicate that a logarithmic profile may be appropriate to describe K_M in this region.

K_M is equal to K^* only at $z = 1.45\ h_C$, which is in the middle of the thin inertial sublayer identified from the mean longitudinal velocity profile (Figures 2a, 3a) between $z = 1.35\ h_C$ and $z = 1.55\ h_C$. Above $1.45\ h_C$, K_M is approximately constant, and we do not find a well defined inertial layer in which K_M matches K^*. This is similar to the results from wind tunnel experiments (Raupach et al., 1986; Brunet et al., 1994). Raupach et al. (1986) suggest that the inertial sublayer is 'squeezed out' between the roughness sublayer and an outer layer in which K_M is independent of z, and interpret this as a consequence of the high value of h_C/δ (δ is boundary-layer depth) in their wind tunnel experiments compared with the atmospheric boundary layer and most other laboratory rough-wall boundary-layer flows. Similarly, we attribute the constant K_M above $1.45\ h_C$ from our LES to the limited vertical domain which extends only to three times the canopy height.

The short dashed line inside the forest in Figure 9a is the eddy diffusivity parameterized as $L\sigma_{\langle w \rangle}$ (Goudriaan, 1977), where the mixing length L is set to 3.1 m, and the standard deviation of the resolved-scale vertical velocity $\sigma_{\langle w \rangle}$ is directly estimated from the LES output (Figure 6a). It demonstrates that this simple parameterization with a single length scale describes the eddy diffusivity quite well in a shear-driven flow within the forest since both K_M (Figure 9a) and $\sigma_{\langle w \rangle}$ (Figure 6a) increase approximately linearly with height within the forest.

In Figure 9b, it is shown that the turbulent Schmidt number, i.e., the ratio K_M/K_χ, is between 0.55 and 0.86, except for the first grid from the soil surface. Inside the forest, the averaged value of K_M/K_χ is about 0.61, while the averaged value of K_M/K_χ between h_C and $2\ h_C$ is about 0.77.

4.2. SPECTRA AND COSPECTRA

One-dimensional spectra and cospectra with respect to wavenumber in the y-direction k_y (Figure 10), are obtained by first performing a horizontal two-dimensional Fast Fourier Transform (FFT) and then summing up amplitudes of all wavenumbers in the x-direction, similar to Moeng and Wyngaard (1988). Spectra and cospectra with respect to the natural frequency f (Figure 11) are estimated from single-point time series using an FFT. The one dimensional wavenumber and natural frequency are defined as $k_y = 1/L_y$ and $f = 1/T$, respectively, where L_y is the corresponding wavelengths in meters, and T is the time period in seconds. In addition, each 30-min period of 10 Hz data from field measurements is block averaged to 1 Hz and cut into three 20-min periods with 5-min overlap to obtain a similar range of frequencies of the spectra and cospectra as the time series from LES.

In Figure 10, it is shown that the normalized spectra and cospectra with respect to the normalized wavenumber in the y-direction κ_y have slopes close to the inertial subrange values of $-2/3$ and $-4/3$, respectively, although the slopes become
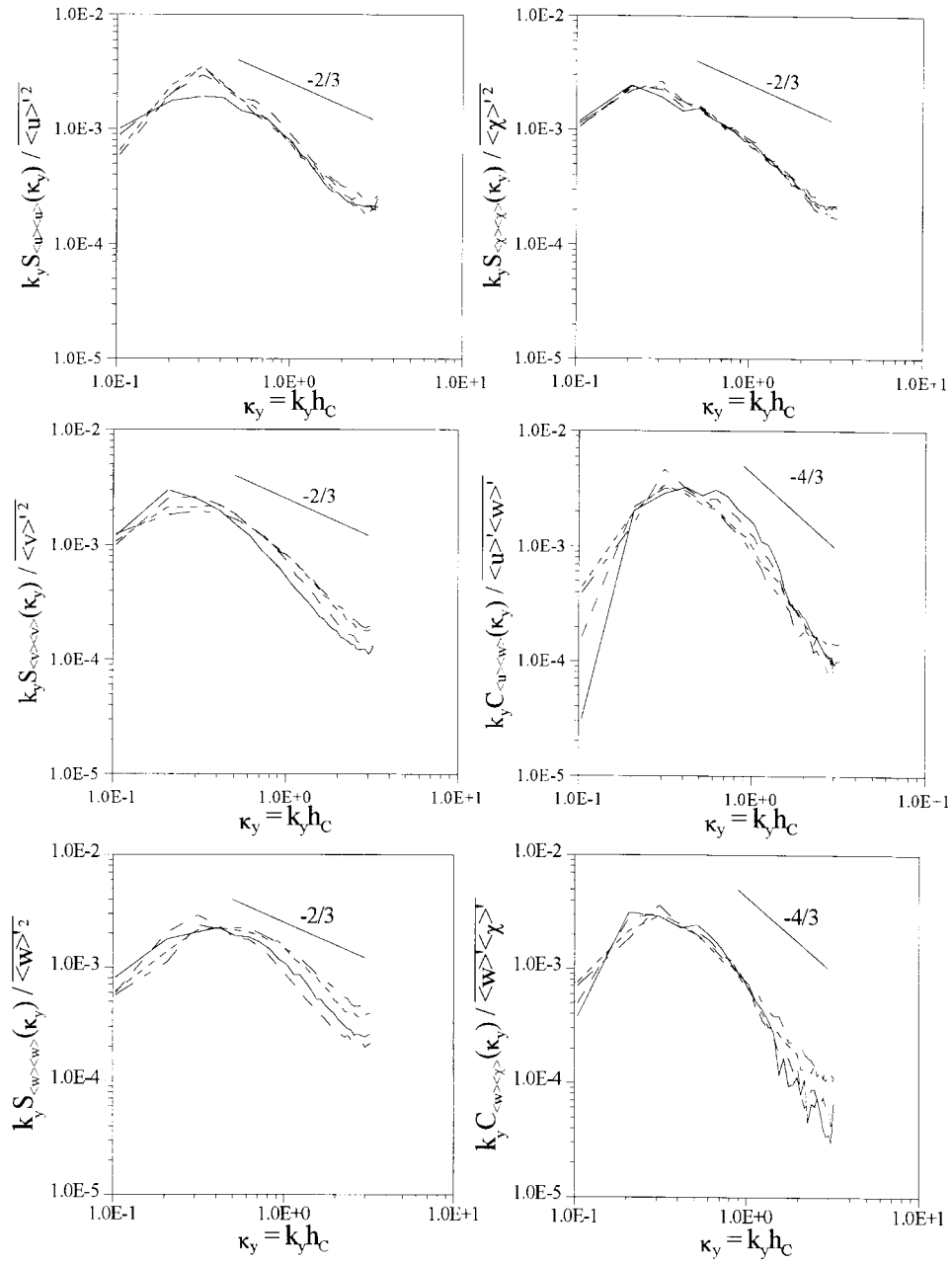
Figure 10. Normalized spectra and cospectra with respect to normalized wavenumber in the y-direction κ_y at $z/h_C = 0.35$ (solid curve), 0.55 (long dashed curve), 0.95 (short dashed curve) and 1.95 (long-short-dashed curve) from the LES.
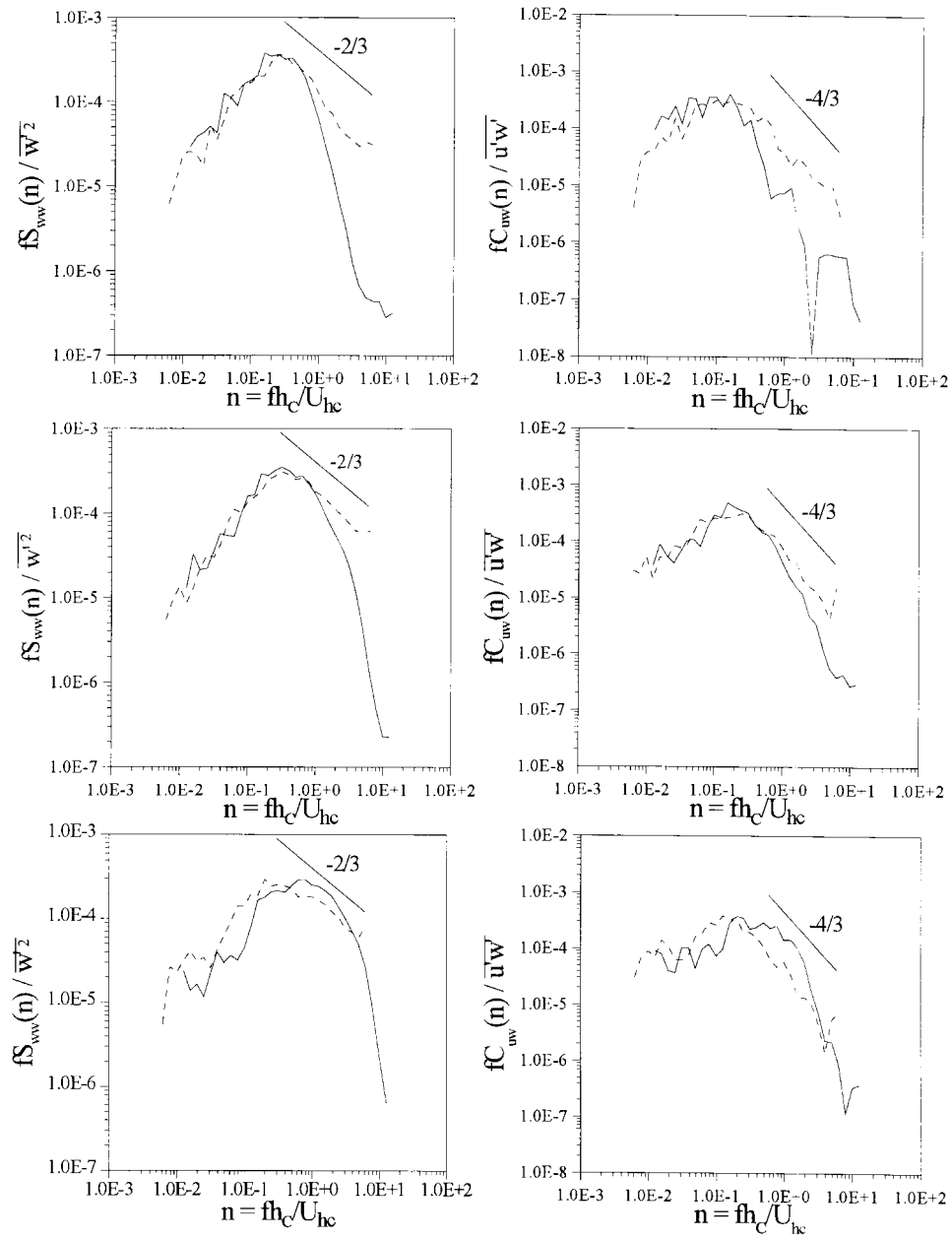
Figure 11. Normalized spectra of vertical velocities (left) and normalized cospectra between vertical velocity and longitudinal velocity (right) from the LES (solid curve) and observation (dashed curve) with respect to normalized natural frequency n at $z/h_C = 0.55$, 0.95 and 1.95 for LES, and at $z/h_C = 0.60$, 1.0 and 1.94 for observation (from top down).

steeper when κ_y is greater than 1.0 or wavelength L_y is smaller than the canopy height h_C. Spectra and cospectra of velocities at $z/h_C = 0.35$ and 0.55 seem to have steeper slopes than those at $z/h_C = 0.95$ and 1.95 by about -0.2. Baldocchi and Meyers (1988) showed that within the tree crown, the measured spectra in the band of wavenumbers associated with the inertial subrange, had a slope of -1.3. They indicated that the steeper spectral slope might be evidence of a short-circuit of the inertial cascade, which is more likely to happen within a tall canopy, such as a forest, because the shear generated turbulence has much larger scales than the wake motions. Although we assume Kolmogorov's inertial-subrange spectral slope of $-5/3$ in the derivation of the coefficients c_e and c_K to parameterize the viscous dissipation ϵ and SGS eddy diffusivity $\langle K_M \rangle$, the drag force directly acts on all resolved-scale motions in the LES, and is perhaps responsible for the steeper spectral slope within the forest. It is interesting to see that the scalar spectra at all heights collapse much better than the velocity spectra and have the same slope both above and within the forest. This may be additional evidence that the drag force has a more direct effect on the velocity field than the scalar field, and is responsible for the steeper slope of the velocity spectra within the forest.

In Figure 11, it is demonstrated that the normalized spectra and cospectra with respect to the normalized frequency n from the observation have slopes close to $-2/3$ and $-4/3$ in the inertial subrange, respectively. Only the spectra of vertical velocity at $z/h_C = 0.60$ show steeper slopes. The slopes of the normalized spectra and cospectra from LES at $z/h_C = 1.95$ match those of the observation at $z/h_C = 1.94$ quite well, and only become much steeper than the observation when n is larger than that of observations. The range of n in which normalized spectra and cospectra from the LES match observations decreases with depth into the forest, or the slopes become much steeper than observation at a lower normalized frequency n with increasing depth into the forest. In addition, for the same height within the forest, the slopes of the spectra and cospectra at the highest frequencies (Figure 11) from LES are even more negative than the slopes of corresponding spectra and cospectra at the highest wavenumbers (Figure 10). These two facts suggest that within the forest, smaller scale eddies might move at a local wind speed, which is smaller than the translation speed (close to wind speed at and above the forest), at which the larger scale eddies are convected downwind (Shaw et al., 1995). Therefore, this raises another challenging question in the use of Taylor's hypothesis even if one selects the right convective velocity for the larger eddies, because it is likely that the convective/translation velocity itself is a function of the scale of motions being convected along. For example, in a study of grid-generated decaying turbulence, Comte-Bellot and Corrsin (1971) found it necessary to apply a wavenumber-dependent translation velocity to define a time scale for convection by larger eddies.

4.3. QUADRANT AND CONDITIONAL ANALYSIS

Quadrant analysis partitions the momentum flux into four quadrants. Quadrants 1 and 3 represent upward transfer of momentum by updrafts of fast air parcels ($\langle u \rangle' > 0$ and $\langle w \rangle' > 0$) and downdrafts of slow air parcels ($\langle u \rangle' < 0$ and $\langle w \rangle' < 0$), and are termed 'outward interaction' and 'inward interaction', respectively. On the other hand, quadrants 2 and 4 correspond to downward transfer of momentum by updrafts of slow air parcels ($\langle u \rangle' < 0$ and $\langle w \rangle' > 0$) and downdrafts of fast air parcels ($\langle u \rangle' > 0$ and $\langle w \rangle' < 0$), and represent the so-called 'ejection or burst' and 'sweep or gust' motions, respectively. Here we apply quadrant analysis with horizontal averaging to the resolved-scale momentum and scalar transport using LES field, while time averaging is used with measurements.

In Figure 12a-1, both LES and observation shows that, above the canopy, the downward flux of momentum contributed by sweep and ejection quadrants each has a magnitude of about 60% of the net downward momentum flux. However, sweeps transport more momentum down into the forest than ejections. The upward transport of momentum by outward and inward interactions has a similar magnitude of about 10% of the net downward momentum flux, but their magnitudes increase with depth into the forest and become equally important as sweep and ejections near the forest floor. In addition, observation shows larger fraction of percentage of each quadrant than LES. Similar features are also shown in Figure 12b-1 regarding the vertical transport of scalar, where quadrants 1 and 3 represent upward transfer of scalar by updrafts of higher concentration parcels ($\langle \chi \rangle' > 0$ and $\langle w \rangle' > 0$) and downdrafts of lower concentration parcels ($\langle \chi \rangle' < 0$ and $\langle w \rangle' < 0$); while quadrants 2 and 4 correspond to downward transfer of scalar by updrafts of lower concentration parcels ($\langle \chi \rangle' < 0$ and $\langle w \rangle' > 0$) and downdrafts of higher concentration parcels ($\langle \chi \rangle' > 0$ and $\langle w \rangle' < 0$), respectively. Above the forest, quadrants 1 and 3 each accounts for about 60% of the net upward scalar flux, and quadrant 3 becomes more important than quadrant 1 within the canopy. In addition, downward scalar fluxes contributed by quadrant 2 and quadrant 4 are about 13% and 7% of the net upward scalar flux, respectively.

In Figure 12a-2, it is illustrated that sweeps occupy a smaller area or a shorter period of time than ejections, especially inside the forest. In addition, sweeps and ejections occur over a larger portion of the total horizontal area or over a larger fraction of time than do outward and inward interactions. This is a reflection of strong negative correlation between $\langle u \rangle'$ and $\langle w \rangle'$. Similar features are also shown in Figure 12b-2 for the scalar transport.

Once again, Figure 13a shows that sweeps and ejections are about equal in downward transport of momentum above the canopy, but sweeps are more important than ejections within the canopy, especially in the upper half of the forest. In addition, observation shows larger ratios of the momentum flux by sweeps to that by ejections. Similar features are also shown in Figure 13b for the upward transport of scalar by quadrants 3 and 1.
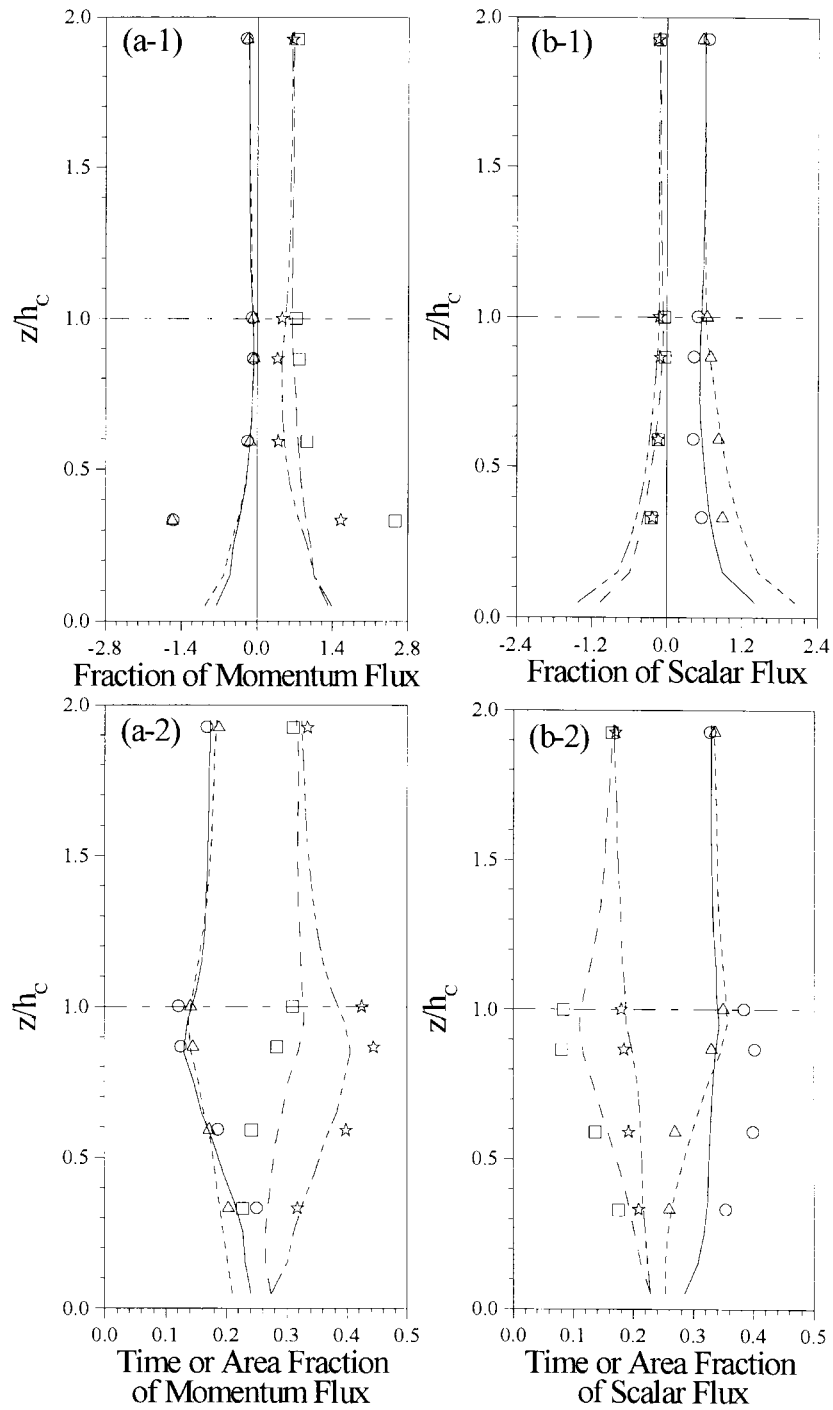
Figure 12. Quadrant partitions of (a-1) momentum flux; (a-2) area or time fraction of each quadrant for momentum flux; (b-1) and (b-2) are the same as (a-1) and (a-2) but for scalar transport. Quadrant 1: solid curve or circle; Quadrant 2: dot-dashed curve or star; Quadrant 3: short dashed curve or triangle; Quadrant 4: long dashed curve or square. Curves are from the LES using horizontal averaging, and points are from the observation using time averaging.
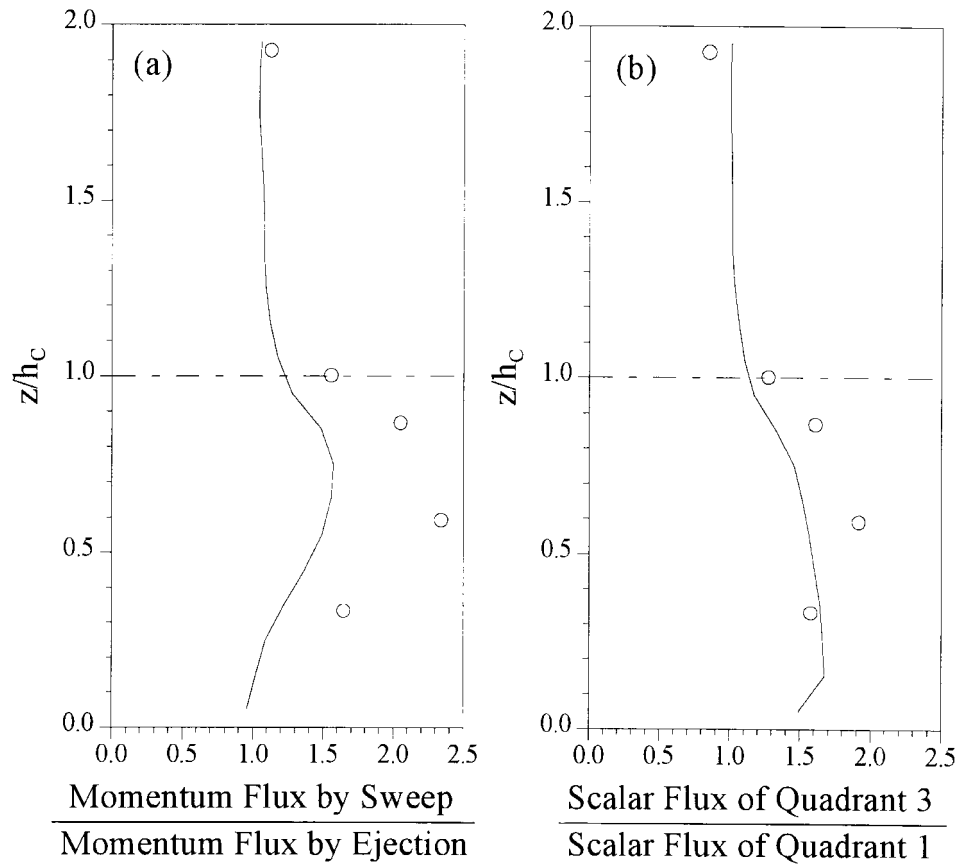
Figure 13. Flux ratio: (a) momentum flux by sweep to that by ejection; (b) scalar flux by quadrant 3 to that by quadrant 1; Curves are from the LES and points are from the observation.

Conditional sampling is often used to evaluate the intermittency of turbulent flow (Shaw and Tavangar, 1983; Raupach et al., 1986), viz.

$$\overline{\langle u \rangle' \langle w \rangle'}(H) = \frac{1}{N} \sum_{i=1}^{N} \langle u \rangle' \langle w \rangle' I(i) \tag{15}$$

where i represents a single point in time or space, N the total number of points; the conditioning function $I(i)$ is equal to 1 if $|\langle u \rangle' \langle w \rangle'| \geq H |\overline{\langle u \rangle' \langle w \rangle'}|$, otherwise $I(i)$ is set to zero. The overbar denotes an average over time or horizontal plane. The nondimensional quantity H is a measure of intermittency called the hole size. A larger value of H indicates more importance of an intermittent event (sweep/ejection) that has a greater magnitude of $\langle u \rangle' \langle w \rangle'$. Accordingly, the portion of the horizontal area or time of the motions that contribute to the conditionally sampled momentum flux for a given H value is calculated. The same procedure is used to calculate scalar flux.
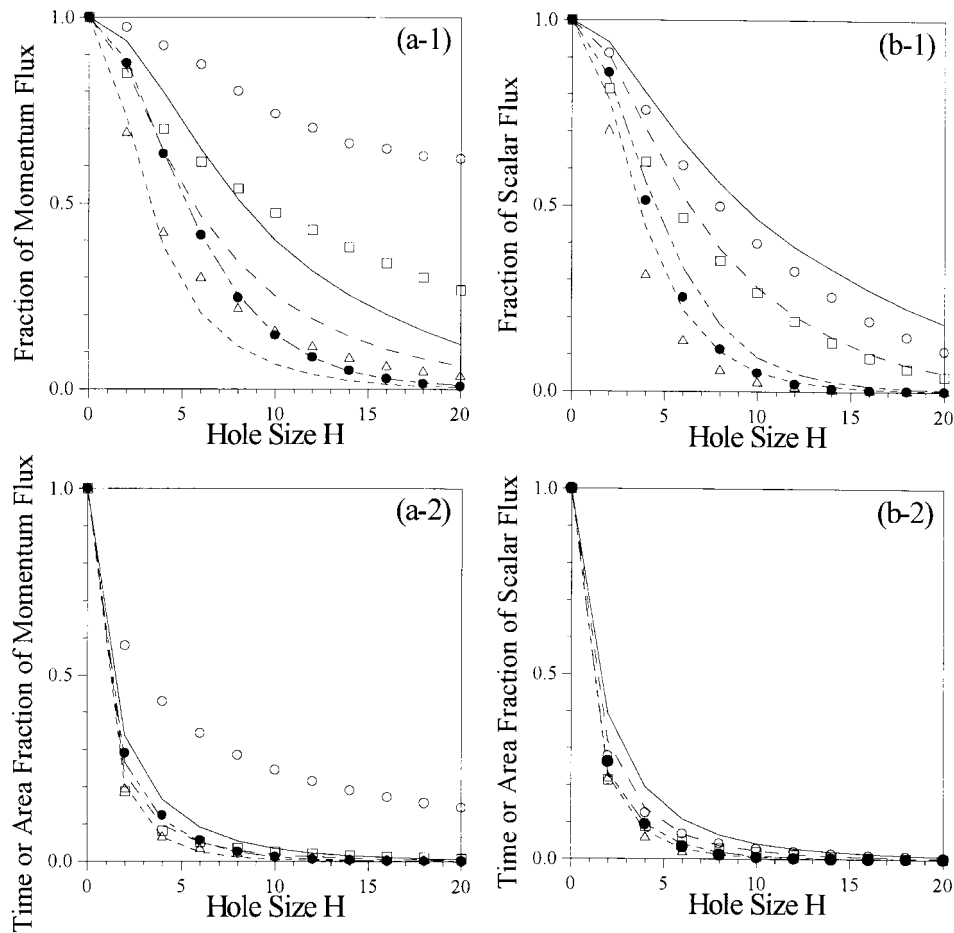
Figure 14. Variations of (a-1) momentum flux fraction and (a-2) area or time fraction with hole size H; (b-1) and (b-2) are similar to (a-1) and (a-2) but for the scalar flux. Curves are from the LES at $z/h_C = 0.35$ (solid), 0.55 (long dashed), 0.95 (short dashed) and 1.95 (dot dashed), while points are from observation at $z/h_C = 0.34$ (open circle), 0.60 (open square), 1.0 (open triangle) and 1.94 (solid circle).

It is shown in Figure 14 that the ratios of the conditionally sampled momentum and scalar fluxes decrease with increasing hole size H much more slowly than the portion of the area or time of which the turbulent motions contribute to the corresponding fluxes. This is the case at all heights within and above the forest. It implies that relatively large fractions of the momentum and scalar fluxes occur over relatively small portions of the area or over short period of time. This indicates the intermittent characteristic of the flow fields within and above the forest. Both LES and observation illustrate that the flux fractions decrease more slowly with depth into the forest, implying increasing intermittency of the turbulent transport with depth into the forest.
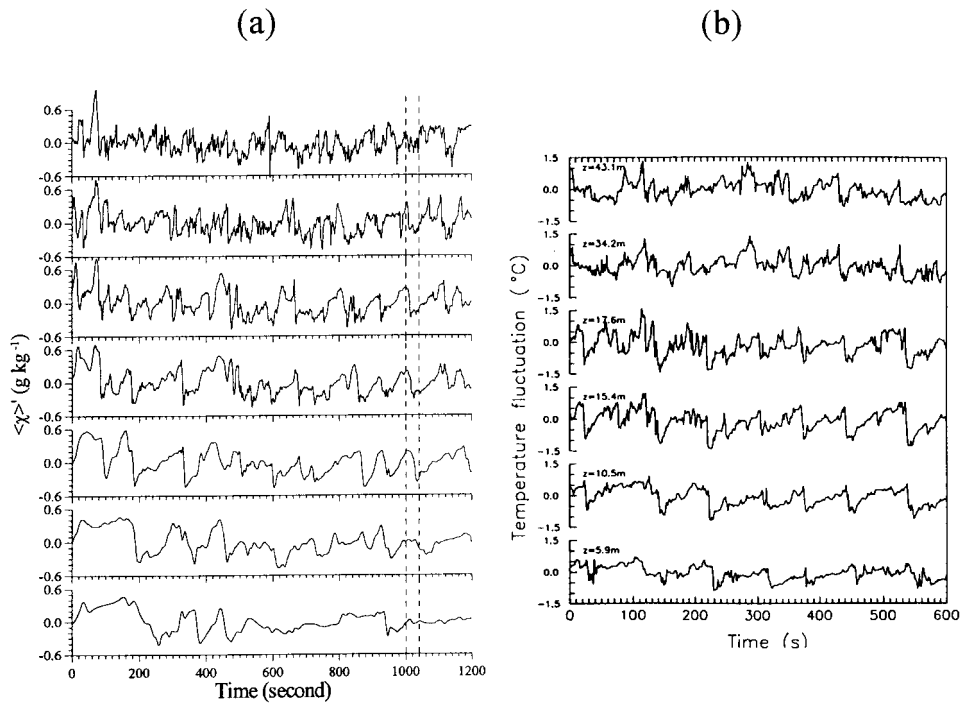
Figure 15. Time series of (a) fluctuating scalar from the LES at $z/h_C = 1.95, 1.45, 0.95, 0.75, 0.55$, 0.35 and 0.15 (from top down); and (b) temperature fluctuations from the observation (after Gao et al., 1989), where the top of the canopy is at $z = 18$ m.

4.4. SIGNATURES OF COHERENT STRUCTURES

A comprehensive analysis of the characteristics of coherent structures is beyond the scope of this paper. Here we show some signatures of the coherent structures from the LES and compare them with previous tower-based measurements over a deciduous forest (Gao et al., 1989; Shaw et al., 1990; Zhuang and Amiro, 1994).

Illustrated in Figure 15a are well defined ramp patterns in the time series of fluctuating scalar concentration $\langle \chi \rangle'$ at various heights both within and above the forest for the same horizontal location (ix, iy) from the LES. These ramp structures have varying amplitude, duration and separation between ramps, and the largest durations are on the order of 130 s, comparable with observation of Gao et al. (1989) (Figure 15b). Both LES and observation show that the sharp drops in scalar concentration or temperature at a lower level lags those at a higher level. An example of the ramp structure from the LES has been marked with two dashed lines in Figure 15a. In addition, less higher frequency fluctuations are observed with depth into the forest from both LES and observation, although the time series from the LES seem to be smoother within the forest.
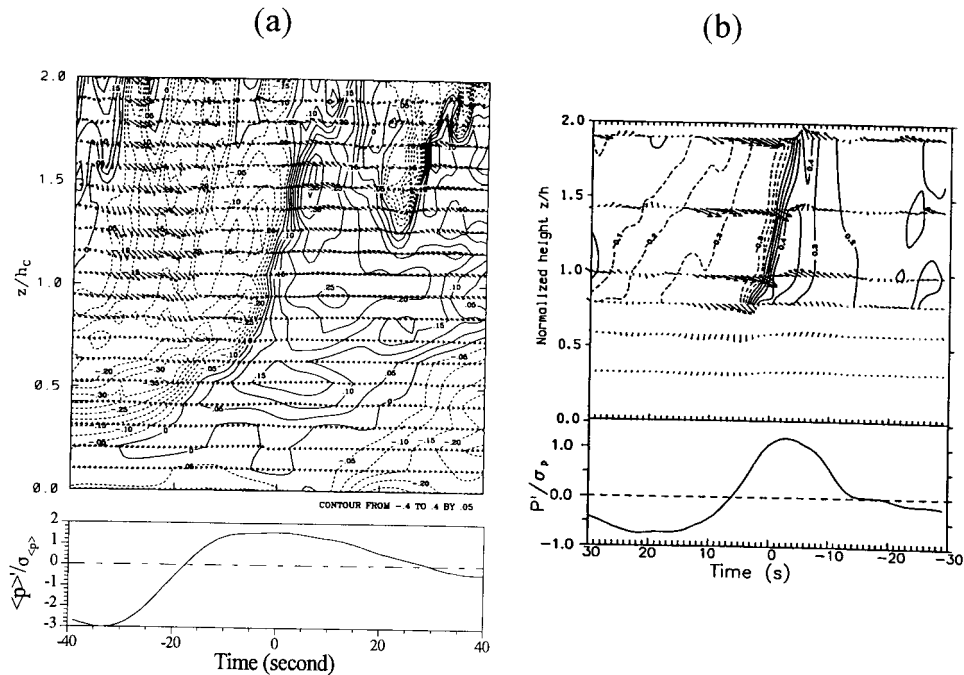
Figure 16. (a) Upper diagram: height-time cross-section contours of the fluctuating scalar $\langle\chi\rangle'$ and wind vectors ($\langle u\rangle'$, $\langle w\rangle'$) (maximum fluctuating wind vector corresponds to 1.5 m s^{-1}). The local time averages have been subtracted. Solid contours are positive and dashed contours are negative, and the first solid contour from the dashed contours represents the zero contour level. Lower diagram: corresponding time series of static pressure perturbations normalized by the local standard deviation of the 20-min period at $z/h_C = 0.05$; and (b) similar to (a) but the observation and the contours are of humidity fluctuations (after Shaw et al., 1990).

Using the time series saved at the same x, y location from the LES, we have plotted a height-time cross-section of the contours of fluctuating scalar $\langle\chi\rangle'$ and wind vector ($\langle u\rangle'$, $\langle w\rangle'$) in Figure 16a for the 80-s period from 970 to 1050 s, in a manner similar to Gao et al. (1989) and Shaw et al. (1990), where the local time averages have been subtracted, and the time has been reversed to give the impression that the microfront is moving downwind. The clearly defined microfront with sweeps and ejections resembles that shown in Gao et al. (1989) and Shaw et al. (1990) (Figure 16b), for example, the downwind tilt (time lag) of the scalar microfronts. Also included in Figure 16a is the 80-s time series of static pressure perturbations at $z/h_C = 0.05$, which is consistent with pressure measured at the surface in the Camp Borden forest (Shaw et al., 1990) shown in Figure 16b. Both LES and observation show that an overpressure occurs immediately ahead of the microfront.

Figure 17 shows the cross-section of contours of the static pressure perturbation field associated with the scalar microfront and sweep/ejection shown in Figure 16a,
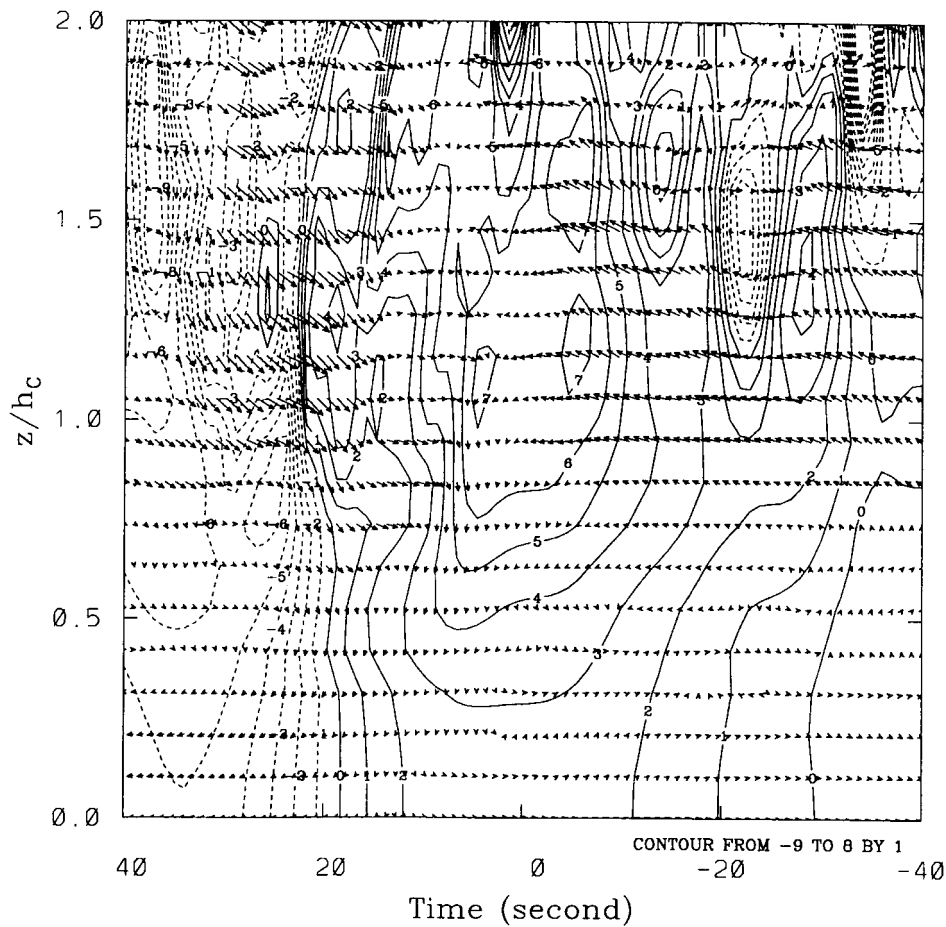
Figure 17. Height-time cross-section contours of the kinematic static pressure perturbations normalized by u_*^2. The wind vectors are the same as in Figure 16a. Solid contours are positive and dashed contours are negative, and the first solid contour from dashed contours represents the zero contour level.

which are quite similar to those retrieved from the velocity and temperature data collected from the Camp Borden deciduous forest (Zhuang and Amiro, 1994), in which a positive pressure perturbation occurs shortly ahead of the microfront, and pressure perturbations appeared to be quite in-phase vertically. However, the negative pressure perturbations in the sweep are much stronger than those shown in Zhuang and Amiro (1994), relative to the positive pressure perturbations ahead.

5. Conclusions

Turbulent statistics of neutrally stratified shear-driven flow within and above a sparse forest canopy have been presented from a large-eddy simulation, and compared with turbulent statistics from turbulence data collected within and above the Camp Borden deciduous forest. In spite of the limited domain size and the coarse grid resolution used in the LES, the turbulent statistics of the simulated flow are in good agreement with the observations, especially the first- and second-order moments. Although the third-order moments from the LES demonstrate the same vertical patterns as those from observation, LES yields smaller magnitudes within the forest. This could be improved by finer grid resolution and a more extent numerical domain. We conclude that LES is a practical tool to study the characteristics and dynamics of turbulent flow within and above plant canopies, and to evaluate and improve existing ensemble average models applied to flows in such regimes.

The addition of an artificial sink of the scalar and a source of momentum in the top layer of the model domain conserves the scalar concentration and momentum in the entire numerical domain, and serves to obtain steady-state statistics. In addition, they also serve to simulate a constant flux layer, which is close to the observed quasi-constant flux profiles in the surface layer above plant canopies.

The SGS parameterization constant used in Moeng (1984) needs to be modified inside the forest due to the pressure/form drag production of subgrid kinetic energy. This modification appears to be important to simulate the inertial subrange spectra with slopes close to those from measurements.

Signatures of coherent structures and their importance in the transport of momentum and mass within and above the forest from the LES also resemble field observations. More systematic and detailed analysis of the eddy characteristics must be performed to obtain a better understanding of their relation to turbulent transport within and above plant canopies.

Finally, the effects of a more extensive model domain, finer grid resolution, various background flows and external driving forces, various leaf densities and thermal stratification on the turbulent statistics and flow structures within and above a forest canopy remain to be further pursued. Effects of the grid resolution and the vertical domain on the magnitudes of the third-order moments are important because these higher moments are needed in evaluating the budget and closure schemes in higher-order closure models.

Acknowledgment

Monique Y. Leclerc for her support in accomplishing the final revision of the manuscript. Comments from two anonymous reviewers are also appreciated.

References

Amiro, B. D.: 1990, 'Drag Coefficients and Turbulence Spectra within Three Boreal Forest Canopies', *Boundary-Layer Meteorol.* **52**, 227–246.

Andrén, A., Brown, A. R., Graf, J., Mason, P. J., Moeng, C.-H., Nieuwstadt, F. T. M. and Schumann, U.: 1994, 'Large-Eddy Simulation of a Neutrally Stratified Boundary Layer: A Comparison of Four Computer Codes', *Quart. J. Roy. Meteorol. Soc.* **120**, 1457–1484.

Baldocchi, D. D. and Meyers, T. P.: 1988, 'A Spectral and Lag-Correlation Analysis of Turbulence in a Deciduous Forest Canopy', *Boundary-Layer Meteorol.* **45**, 31–58.

Brunet, Y., Finnigan, J. J., and Raupach, M. R.: 1994, 'A Wind Tunnel Study of Air Flow in Waving Wheat: Single-Point Velocity Statistics', *Boundary-Layer Meteorol.* **70**, 95–132.

Cionco, R. M.: 1965, 'A Mathematical Model for Air Flow in a Vegetative Canopy', *J. Appl. Meteorol.* **4**, 517–522.

Comte-Bellot, G. and Corrsin, S.: 1971, 'Simple Eulerian Time Correlation of Full- and Narrow-band Velocity Signals in Grid-Generated, 'Isotropic' Turbulence', *J. Fluid Mech.* **48**, 273–337.

Denmead, O. T. and Bradley, E. F.: 1985, 'Flux-Gradient Relationships in a Forest Canopy', in B. A. Hutchison and B. B. Hicks (eds.), *The Forest-Atmosphere Interaction*, D. Reidel Publishing Co., Dordrecht, The Netherlands, pp. 421–442.

Gao, W., Shaw, R., H. and K. T. Paw U: 1989, 'Observation of Organized Structure in Turbulent Flow within and above a Forest Canopy', *Boundary-Layer Meteorol.* **47**, 349–377.

Goudriaan, J.: 1977, *Crop Micrometeorology: A Simulation Study*, Center for Agricultural Publishing and Documentation, Wageningen, The Netherlands, 249 pp.

Inoue, E.: 1963, 'On the Turbulent Structure of Airflow within Plant Canopies', *J. Meteorol. Soc. Japan* **41**, 317–326.

Jackson, P. S.: 1981, 'On the Displacement Height in the Logarithmic Velocity Profile', *J. Fluid Mech.* **111**, 15–25.

Kaimal, J. C. and Finnigan, J. J.: 1994, *Atmospheric Boundary Layer Flows, Their Structure and Measurement*, Oxford University Press, 289 pp.

Kanda, M. and Hino, M.: 1994, 'Organized Structure in Developing Turbulent Flow within and above a Plant Canopy, Using a Large Eddy Simulation', *Boundary-Layer Meteorol.* **68**, 237–257.

Leclerc, M. Y., Beissner, K. C., Shaw, R. H., den Hartog, G., and Neuman, H. H.: 1991, 'The Influence of Buoyancy on Third-Order Turbulent Velocity Statistics within a Deciduous Forest', *Boundary-Layer Meteorol.* **55**, 109–123.

Meyers, T. P and Paw U, K. T.: 1986, 'Testing of a Higher-Order Closure Model for Modeling Airflow within and above Plant Canopies', *Boundary-Layer Meteorol.* **37**, 297–311.

Meyers, T. P and Paw U, K. T.: 1987, 'Modeling the Plant Canopy Micrometeorology with Higher-Order Closure Principles', *Agric. For. Meteorol.* **41**, 143–163.

Moeng, C.-H.: 1984, 'A Large-Eddy-Simulation Model for the Study of Planetary Boundary-Layer Turbulence', *J. Atmos. Sci.* **41**, 2052–2062.

Moeng, C.-H. and Wyngaard, J. C.: 1988, 'Spectral Analysis of Large-Eddy Simulations of the Convective Boundary Layer', *J. Atmos. Sci.* **45**, 3573–3587.

Moeng, C.-H. and Wyngaard, J. C.: 1989, 'Evaluation of Turbulent Transport and Dissipation Closures in Second-Order Modeling', *J. Atmos. Sci.* **46**, 2311–2330.

Newmann, H. H., den Hartog, G., and Shaw, R. H.: 1989, 'Leaf Area Measurements Based On Hemispheric Photographs and Leaf-Litter Collection in a Deciduous Forest During Autumn Leaf-Fall', *Agric. For. Meteorol.* **45**, 325–345.

Patton, E. G., Shaw, R. H., Paw U, K. T. and Moeng, C.-H.: 1994, 'A Comparison of Two Large-Eddy Simulations of Turbulent Flow above and within a Forest Canopy', in preprint for American Meteorological Society *21st Conference on Agricultural and Forest Meteorology & 11th Conference on Biometeorology and Aerobiology*, San Diego, CA, pp. 88–91.

Patton, E. G., Shaw, R. H., and Paw U, K. T.: 1995, 'Large-Eddy Simulation of a Forest: Influence of Canopy Structure on Turbulent Kinetic Energy', in preprint for American Meteorological Society *11th Symposium on Boundary Layers and Turbulence*, Charlotte, NC, pp. 525–528.

Raupach, M. R.: 1979, 'Anomalies in Flux-Gradient Relationships over Forest', *Boundary-Layer Meteorol.* **16**, 467–486.

Raupach, M. R., Coppin, P. A., and Legg, B. J.: 1986, 'Experiments on Scalar Dispersion within a Model Plant Canopy. Part I: The Turbulence Structure', *Boundary-Layer Meteorol.* **35**, 21–52.

Shaw, R. H. and Tavangar, J.: 1983, 'Structure of the Reynolds Stress in a Canopy Layer', *J. Climate Appl. Meteorol.* **22**, 1922–1931.

Shaw, R. H. and Seginer, I.: 1985, 'The Dissipation of Turbulence in Plant Canopies', in preprint for American Meteorological Society *7th Symposium on Turbulence and Diffusion*, Boulder, CO, pp. 200-203

Shaw, R. H. and Seginer, I.: 1987, 'Calculation of Velocity Skewness in Real and Artificial Plant Canopies', *Boundary-Layer Meteorol.* **39**, 315–332.

Shaw, R. H., Den Hartog, G., and Neumann, H. H.: 1988, 'Influence of Foliar Density and Thermal Stability on Profiles of Reynolds Stress and Turbulence Intensity in a Deciduous Forest', *Boundary-Layer Meteorol.* **45**, 391–409.

Shaw, R. H., Paw U, K. T., Zhang, X.-J., Gao, W., den Hartog, G., and Neumann, H. H.: 1990, 'Retrieval of Turbulent Pressure Fluctuations at the Ground Surface Beneath a Forest', *Boundary-Layer Meteorol.* **50**, 319–338.

Shaw, R. H. and Schumann, U.: 1992, 'Large-Eddy Simulation of Turbulent Flow above and within a Forest', *Boundary-Layer Meteorol.* **61**, 47–64.

Shaw, R. H., Brunet, Y., Finnigan, J. J., and Raupach, M. R.: 1995, 'A Wind Tunnel Study of Air Flow in Waving Wheat: Two-Point Velocity Statistics', *Boundary-Layer Meteorol.* **76**, 349–376.

Spalart, P. R., Moser, R. D., and Rogers, M. M.: 1991, 'Spectral Methods for the Navier-Stokes Equations with One Infinite and Two Periodic Directions', *J. Computational Phys.* **96**, 297–324.

Su, H.-B., Paw U, K. T., and Shaw, R. H.: 1996, 'Development of a Coupled Leaf and Canopy Model for the Simulation of Plant-Atmosphere Interactions', *J. Appl. Meteorol.* **35**, 733–748.

Sullivan, P. P., Moeng, C.-H., and McWilliams, J. C.: 1996, 'A Grid Nesting Method for Large-Eddy Simulation of Planetary Boundary-Layer Flows', *Boundary-Layer Meteorol.* **80**, 167–202.

Thom, A. S.: 1971, 'Momentum Absorption by Vegetation', *Quart. J. Roy. Meteorol. Soc.* **97**, 414–428.

Thom, A. S.: 1975, 'Momentum, Mass and Heat Exchange of Plant Communities', in J. L. Monteith (ed.), *Vegetation and the Atmosphere, Volume 1, Principles,* Academic Press, pp. 57–109.

Wilson, N. R. and Shaw, R. H.: 1977, 'A Higher-Order Closure Model for Canopy Flow', *J. Appl. Meteorol.* **16**, 1197–1205.

Zhuang, Y. and Amiro, B. D.: 1994, 'Pressure Fluctuations during Coherent Motions and Their Effects on the Budgets of Turbulent Kinetic Energy and Momentum Flux within a Forest Canopy', *J. Appl. Meteorol.* **33**, 704–711.